NASA CR-145023

THE CALCULATION OF STEADY NON-LINEAR TRANSONIC FLOW OVER FINITE WINGS WITH LINEAR THEORY AERODYNAMICS

By

Atlee M. Cunningham, Jr.

Prepared under Contract No. NAS1-13855

By

GENERAL DYNAMICS CORPORATION
Fort Worth Division
Fort Worth, Texas

for

NASA
National Aeronautics and Space Administration

August 1976

NASA CR-145023

THE CALCULATION OF STEADY NON-LINEAR TRANSONIC FLOW OVER FINITE WINGS WITH LINEAR THEORY AERODYNAMICS

By
Atlee M. Cunningham, Jr.

August 1976

Prepared under Contract No. NAS1-13855 by
GENERAL DYNAMICS CORPORATION
Fort Worth Division
Fort Worth, Texas

for

LANGLEY RESEARCH CENTER
NATIONAL AERONAUTICS AND SPACE ADMINISTRATION

CONTENTS

LIST OF TABLES

LIST OF FIGURES

THE CALCULATION OF STEADY NON-LINEAR TRANSONIC FLOW OVER FINITE WINGS WITH LINEAR THEORY AERODYNAMICS

By Atlee M. Cunningham, Jr.
Fort Worth Division of General Dynamics

SUMMARY

This report documents a study to establish the feasibility of calculating steady mean flow solutions for non-linear transonic flow over finite wings with a linear theory aerodynamic computer program. The methodology is based on independent solutions for upper and lower surface pressures that are coupled through the external flow fields. Two approaches for coupling the solutions are investigated which include the diaphragm and the edge singularity method. The final method is a combination of both where a line source along the wing leading edge is used to account for blunt nose airfoil effects; and the upper and lower surface flow fields are coupled through a diaphragm in the plane of the wing. An iterative solution is used to arrive at the non-uniform flow solution for both non-lifting and lifting cases. Final results for a swept tapered wing in subcritical flow, show that the method converges in three iterations and gives excellent agreement with experiment at $\alpha = 0^{o}$ and 2^{o}. Recommendations are made for development of a procedure for routine application.

SYMBOLS

$[A]$	aerodynamic matrix
$\{a\}$	pressure series coefficients
$C_p = \frac{p-p_\infty}{q_\infty}$	pressure coefficient
c	local wing chord, meters
M_∞, M_ℓ	freestream and local Mach number
p	pressure, Newtons/meter^2

$q_\infty = \frac{\rho U_\infty^2}{2}$	dynamic pressure, Newtons/meter^2
R_{LE}	leading edge "radius", meters
U_∞	freestream velocity, meters/second
u,v,w	velocity components in the x,y,z directions, meters/second
V	total velocity, meters/second
w'	normal wash on surface Z_S
x,y,z	Cartesian coordinates, meters
Z_t	surface thickness coordinate, meters
Z_S	coordinates of the surface induced by the leading edge line source, meters
Z_U, Z_L	upper and lower surface coordinates, meters
$Z'_U = Z_U - Z_S$	meters
$Z'_L = Z_L - Z_S$	meters
α	angle of attack
θ_S	angle of surface Z_S
θ_V	angle of the total velocity component, V

INTRODUCTION

Due to the strong coupling between the oscillatory and steady flow fields in the transonic speed range, it is no longer possible to calculate unsteady aerodynamic forces that are independent of the mean flow field characteristics. A completely adequate transonic aerodynamic method should account for the effects of surface thickness, twist, and camber distribution, mean angle of attack, wing-body and wing-wing interference, mixed flow with imbedded shocks, and boundary layer and boundary layer-shock interaction. Since these effects are embodied in the mean flow fields, they can be accounted for in the unsteady forces in a linear fashion as long as the oscillatory solutions are obtained for small perturbations about the mean flow. Thus, the nonlinearity can be contained within the steady solution which permits linearization of the unsteady solution (ref. 1).

The coupling between steady and unsteady flow fields in the transonic regime has therefore made the calculation of steady state solutions an integral part of the unsteady solution processes used for transonic flutter and dynamic response analyses. As a result, the usual Mach-altitude envelope for flutter clearance must be expanded to a three dimensional Mach-altitude-angle of attack envelope. Mean flow field data could be obtained from either experiment or finite difference solutions. From a practical applications standpoint, however, it would be desirable to have the ability to calculate this data with the same program which is used to calculate the oscillatory solutions. Such a computer program was developed under Contract NAS1-12399 (ref. 1) in which the piecewise linearization concept was applied to steady flow as well as unsteady flow. It appears that this computer program has the potential for developing an economical steady solution which will be suitable as a source of flow field information for calculating oscillatory solutions.

This report documents a study on some candidate modifications to the transonic computer program for providing the capability to calculate steady mean flow solutions. The methodology is based on independent solutions for upper and lower surface pressures which are coupled through the external flow fields. The two methods investigated are the diaphragm and the edge singularity methods. The final method is a combination of both where a line source along the wing leading edge is used to account for blunt nose airfoil effects; and the upper and lower surface flow fields are coupled through a

diaphragm region in the plane of the wing. An iterative solution is used to arrive at the non-uniform flow solution for both non-lifting and lifting cases. Final results for a subcritical case, a swept tapered wing at $M_\infty=0.8$, show that the method converges in three iterations and gives excellent agreement with experiment at $\alpha=0^\circ$ and 2°. Recommendations are made for development of a procedure for routine application.

DEVELOPMENT OF THE METHOD

Two approaches were investigated for the development of a method for coupling linear theory lifting surface solutions together to solve the non-linear thick wing problem. In these approaches, called the diaphragm and edge singularity methods, the upper and lower surfaces of the wing were represented by separate non-interfering lifting surfaces whose induced external flow fields were forced to match off of the wing but only in the same plane of the wing. The boundary conditions required that the upper and lower pressure coefficients and the normal-wash be equal in the interface region. The differences in the two approaches was embodied only in the means by which the external flow field conditions were met. The inadequacy of either method led to the development of a combined approach, the modified diaphragm method, which maintained the best features of both.

In the following paragraphs, the details of the method development will be discussed along with results of the numerical experimentation.

Diaphragm Method

In this method, lifting surfaces on which the free surface boundary conditions are met, are added in such a manner as to surround the wing being considered. The example shown in Figure 1 is the configuration used in this study. The leading and trailing edge diaphragms had three and two chordwise pressure functions, respectively, as compared with eight on the wing. Four spanwise functions were used on all surfaces. Although a tip diaphragm should have been included, it was eliminated for sake of economy. The solution process was identical to that for three wings with mutual interference. The computer program used was that developed under Contract NAS1-12399 (ref. 1).

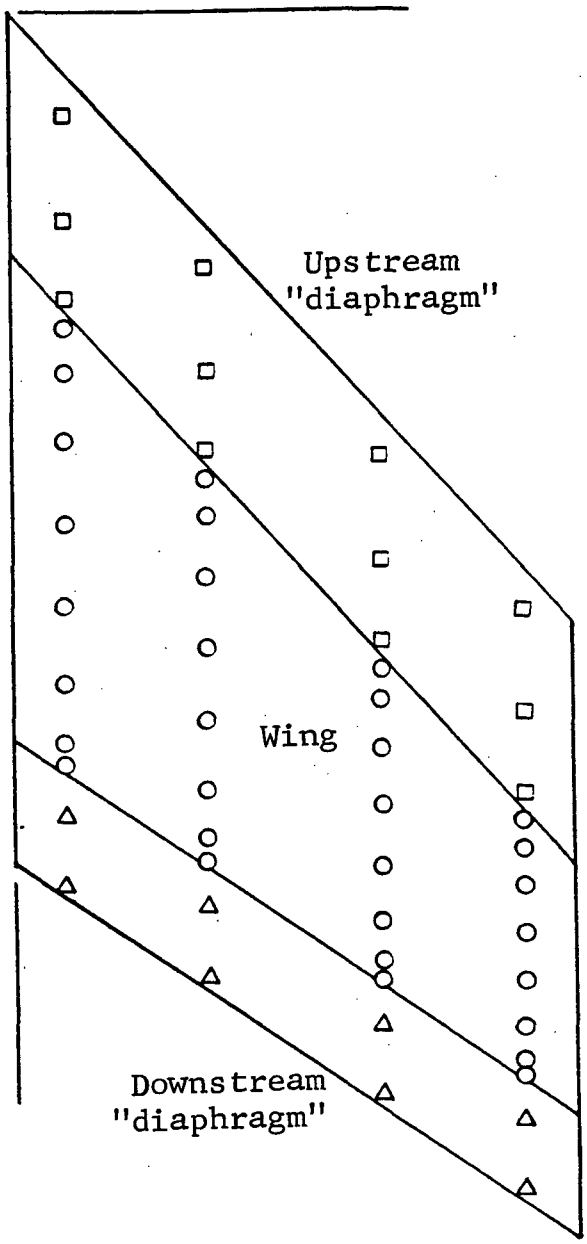

Figure 1.- Geometry and downwash point array for a diaphragm solution for the wing in ref. 2.

For non-lifting cases, only the upper or lower surface need to be considered. The boundary condition met is zero downwash on the diaphragm and surface thickness slopes on the wing. For lifting cases, both the upper and lower surfaces must be considered. The conditions met in the diaphragms are that the downwash and pressure for both upper and lower surfaces are equal in these regions. Flow tangency is satisfied on the upper and lower surfaces of the wing for the corresponding thickness slopes plus or minus the angle of attack, twist, or camber.

The equation applicable to the non-lifting case is a simple interference aerodynamic matrix equation

$$\left[\begin{array}{c|c} A_{DD} & A_{DW} \\ \hline A_{WD} & A_{WW} \end{array}\right] \left\{\begin{array}{c} a_D \\ \hline a_W \end{array}\right\} = \left\{\begin{array}{c} 0 \\ \hline \frac{1}{2}\frac{\partial z_t}{\partial x} \end{array}\right\} \tag{1}$$

where

A_{DD}, A_{DW} = aerodynamic sub matrices for downwash induced on the diaphragm by the diaphragm and wing pressures

A_{WD}, A_{WW} = aerodynamic sub matrices for downwash induced on the wing by the diaphragm and wing pressures

a_D, a_W = pressure function coefficients for the diaphragm and wing

$\frac{\partial z_t}{\partial x}$ = surface thickness slope distribution.

For lifting cases, both upper and lower surface equations are written as

$$\left[\begin{array}{c|c} A^U_{DD} & A^U_{DW} \\ \hline A^U_{WD} & A^U_{WW} \end{array}\right] \left\{\begin{array}{c} a^U_D \\ \hline a^U_W \end{array}\right\} = \frac{1}{2} \left\{\begin{array}{c} w^U_D \\ \hline \frac{\partial z_U}{\partial x} \end{array}\right\} \tag{2a}$$

and

$$\left[\begin{array}{c|c} A^L_{DD} & A^L_{DW} \\ \hline A^L_{WD} & A^L_{WW} \end{array}\right] \left\{\begin{array}{c} a^L_D \\ \hline a^L_W \end{array}\right\} = \frac{1}{2} \left\{\begin{array}{c} w^L_D \\ \hline \frac{\partial z_L}{\partial x} \end{array}\right\} \tag{2b}$$

with the conditions

$$\{a_D^U\} = \{a_D^L\} \tag{3a}$$

$$\{w_D^U\} = -\{w_D^L\} \tag{3b}$$

From equation 3a, a simplification is possible since

$$[A_{DD}^L] = [A_{DD}^U] \tag{4}$$

Thus from equations 2, 3b, and 4, the lifting equations become

$$\begin{bmatrix} 2A_{DD} & A_{DW}^U & A_{DW}^L \\ \hline A_{WD}^U & A_{WW}^U & 0 \\ \hline A_{WD}^L & 0 & A_{WW}^L \end{bmatrix} \begin{Bmatrix} a_D \\ \hline a_W^U \\ \hline a_W^L \end{Bmatrix} = \frac{1}{2} \begin{Bmatrix} 0 \\ \hline \frac{\partial z_U}{\partial x} \\ \hline -\frac{\partial z_L}{\partial x} \end{Bmatrix} \tag{5}$$

The terms z_U and z_L are the surface thickness coordinates as modified by angle of attack, camber, or twist. Although equation 5 can be reduced by the number of rows and columns corresponding to $\{a_D\}$, it is more convenient to retain this form for purposes of iteration. If core storage becomes critical, then the reduced form can be used as follows:

$$\begin{bmatrix} A_W^U - \frac{A_{WD}^U A_{DD}^{-1} A_{DW}^U}{2} & -\frac{A_{WD}^U A_{DD}^{-1} A_{DW}^L}{2} \\ \hline -\frac{A_{WD}^L A_{DD}^{-1} A_{DW}^U}{2} & A_{WW}^L - \frac{A_{WD}^L A_{DD}^{-1} A_{DW}^L}{2} \end{bmatrix} \begin{Bmatrix} a_W^U \\ \hline a_W^L \end{Bmatrix} = \frac{1}{2} \begin{Bmatrix} \frac{\partial z_U}{\partial x} \\ \hline \frac{\partial z_L}{\partial x} \end{Bmatrix} \tag{6}$$

For purposes of this study, equation 5 was used throughout.

The effect of the diaphragm is illustrated in Figure 2 where a non-lifting case is considered for the wing configuration shown in Figure 1. The airfoil section is a NACA 64A010 profile normal to the 45° swept quarter chord axis of the wing. Experimental pressure distributions on both upper and lower surfaces are available in ref. 2 for a range of Mach numbers and angles of attack. The solid line is the midspan solution with leading and trailing edge diaphragms for the surface thickness slopes. The flow is uniform over all surfaces at $M_\ell = M_\infty = 0.8$. The dashed line is the same solution with the diaphragms removed. The symbols are experimental data. In comparing these results with experiment, it is clear that the diaphragm concept provides a significant improvement, particularly toward the trailing edge. The leading edge region, however, is not greatly improved due to the fact that very high order functions are still needed to represent the surface thickness slopes near the leading edge where they become singular for a blunt nose airfoil.

Edge Singularity Method

The two-fold purpose of this method is to achieve the same result as the diaphragm method with less cost and storage requirement, and improve the leading edge representation. The concept is basically the same with exception that the diaphragm regions are replaced with singularities along the edge of the wing. The boundary conditions are:

(1) Stagnation flow at the leading edge (which is satisfied by a line source along the leading edge);

(2) A downwash discontinuity at the leading edge between the upwash and mean camber line slope (which is satisfied by a line doublet also along the leading edge);

(3) Flow tangency along the upper and lower surfaces (as satisfied by conventional pressure distributions);

(4) Zero pressure coefficient differential along the trailing edge and streamwise tip; and

(5) Zero downwash differential just aft of the trailing edge and outboard of the streamwise tip.

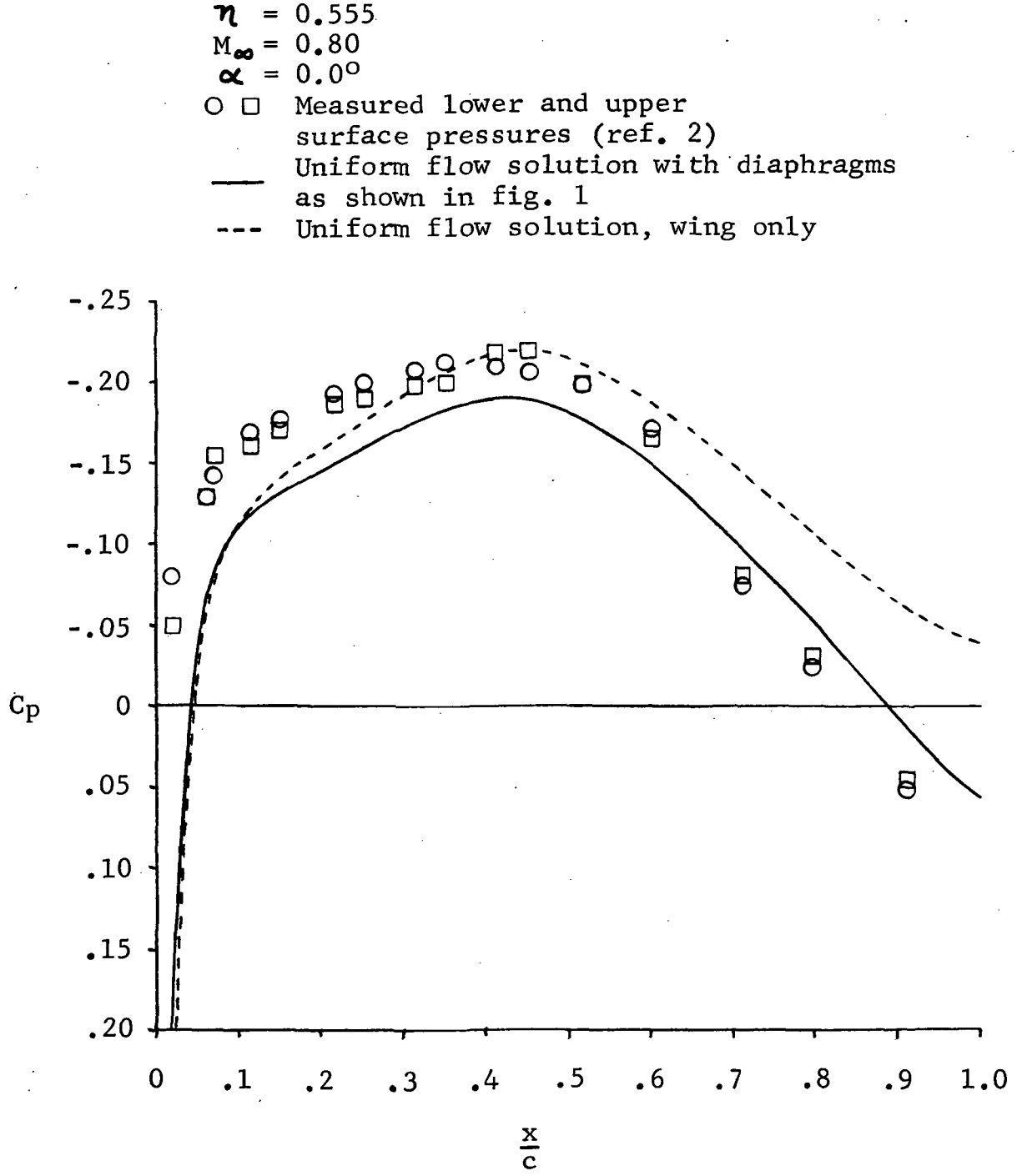

Figure 2.- Effect of the diaphragms on the uniform flow solution for surface thickness slopes.

Items 4 and 5 are met with either doublets along the trailing edge (one on the upper and one on the lower surfaces) or one additional pressure term in both the upper and lower surface pressure functions.

An illustrative example for application of the leading edge line source is shown in Figure 3. The line source is placed at an appropriate point from which stagnation flow is achieved at the leading edge. The strength of the line source is determined for the free stream conditions and planform geometry, and is held constant throughout the analysis for all values of α. The body surface generated by the line source, z_s, as indicated by the dashed line, is subtracted from the airfoil coordinates, z_u and z_L. This step yields the modified upper and lower surface coordinates, z_u' and z_L', which no longer have singular slopes at the leading edge.

A more specific example is shown in Figure 4 where the airfoil section (NACA 64A010 profile swept at 45°, ref. 2) is treated with the leading edge line source. The modified surface, $z_t' = z_t - z_s$, now appears more like a sharp edged airfoil. Likewise, the modified slopes no longer tend toward a strong singularity. The value of the leading edge radius parameter, $R_{LE} = 0.005c$, was chosen from graphical considerations.

Equations for applying the leading edge line source model are developed and presented in the appendix. These equations were coupled with the diaphragm method to determine the effect of varying the parameter, R_{LE}. A diaphragm solution was developed at $M_\infty = 0.8$ for the wing shown in Figure 1 where the Mach number distribution for non-uniform flow was obtained from the experimental data in ref. 2. The effect of varying R_{LE} in this solution is shown in Figure 5. The solution for the graphically determined value, $R_{LE} = 0.005c$, is the best of those shown, however, $R_{LE} = 0.004c$ would have been slightly better. More important, these results imply that the leading edge line source coupled with thin wing lifting surface solutions appears to provide a realistic tool for solving 3-D thick wing problems.

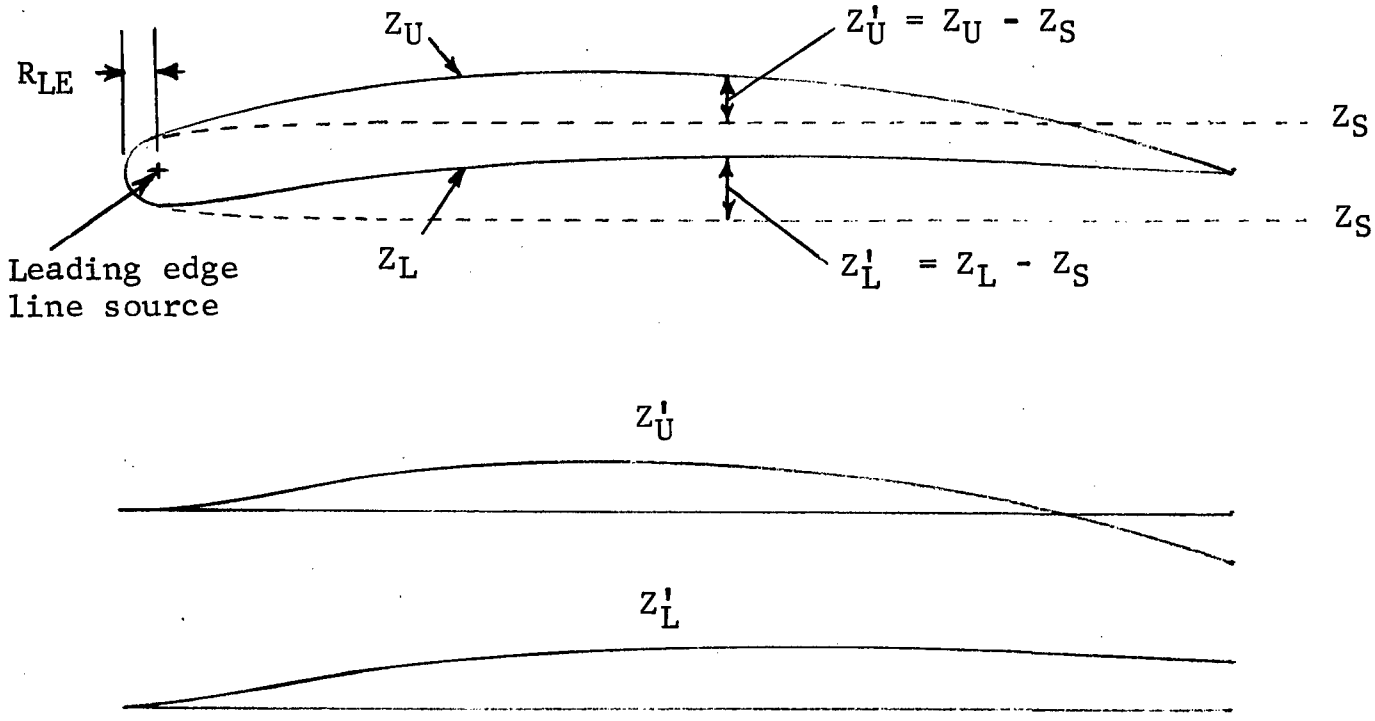

Figure 3.- Decomposition of a blunt nose airfoil section

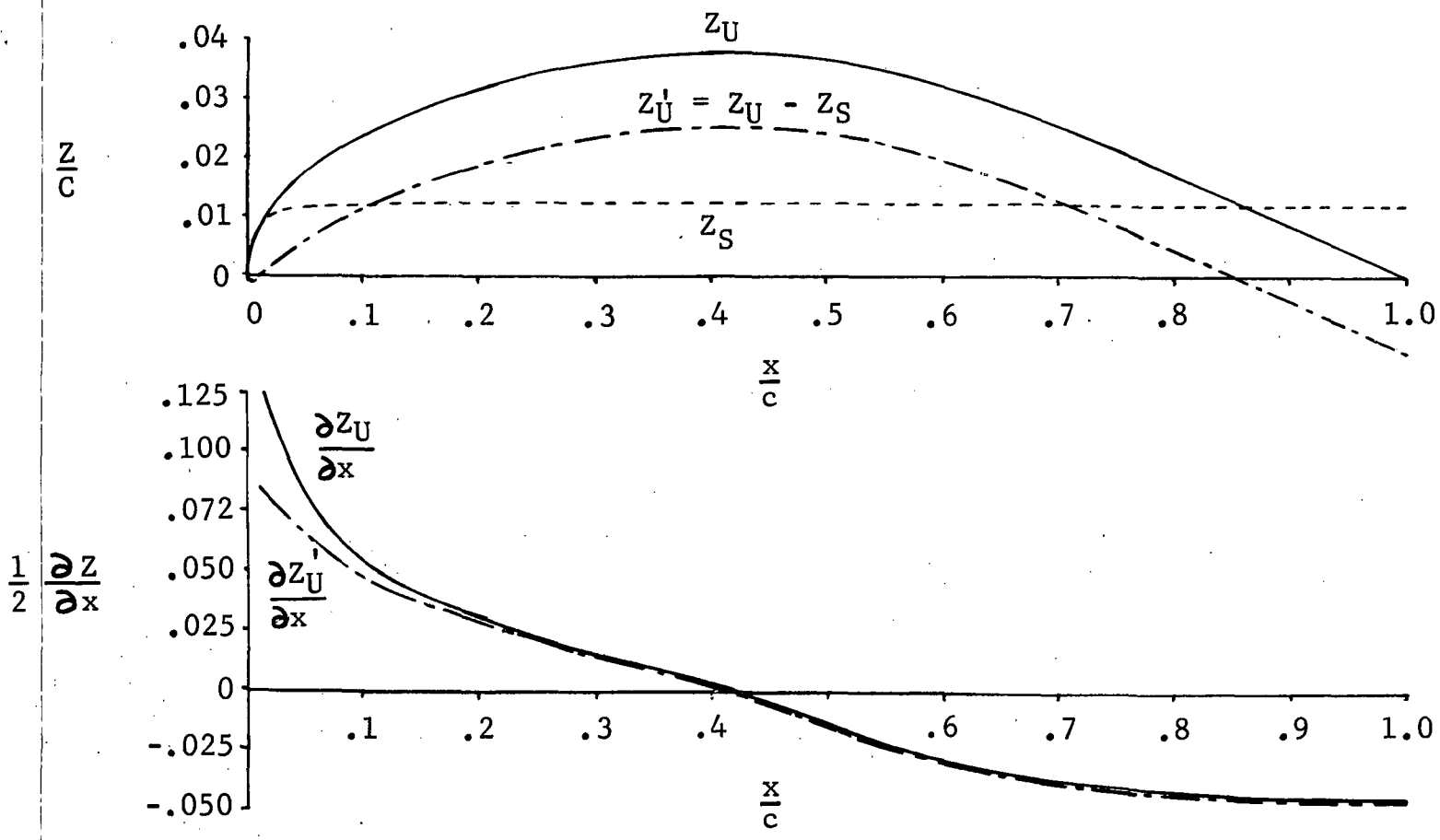

Figure 4.- Decomposition of the airfoil section of ref. 2 (NACA 64A010, sweep = 45°).

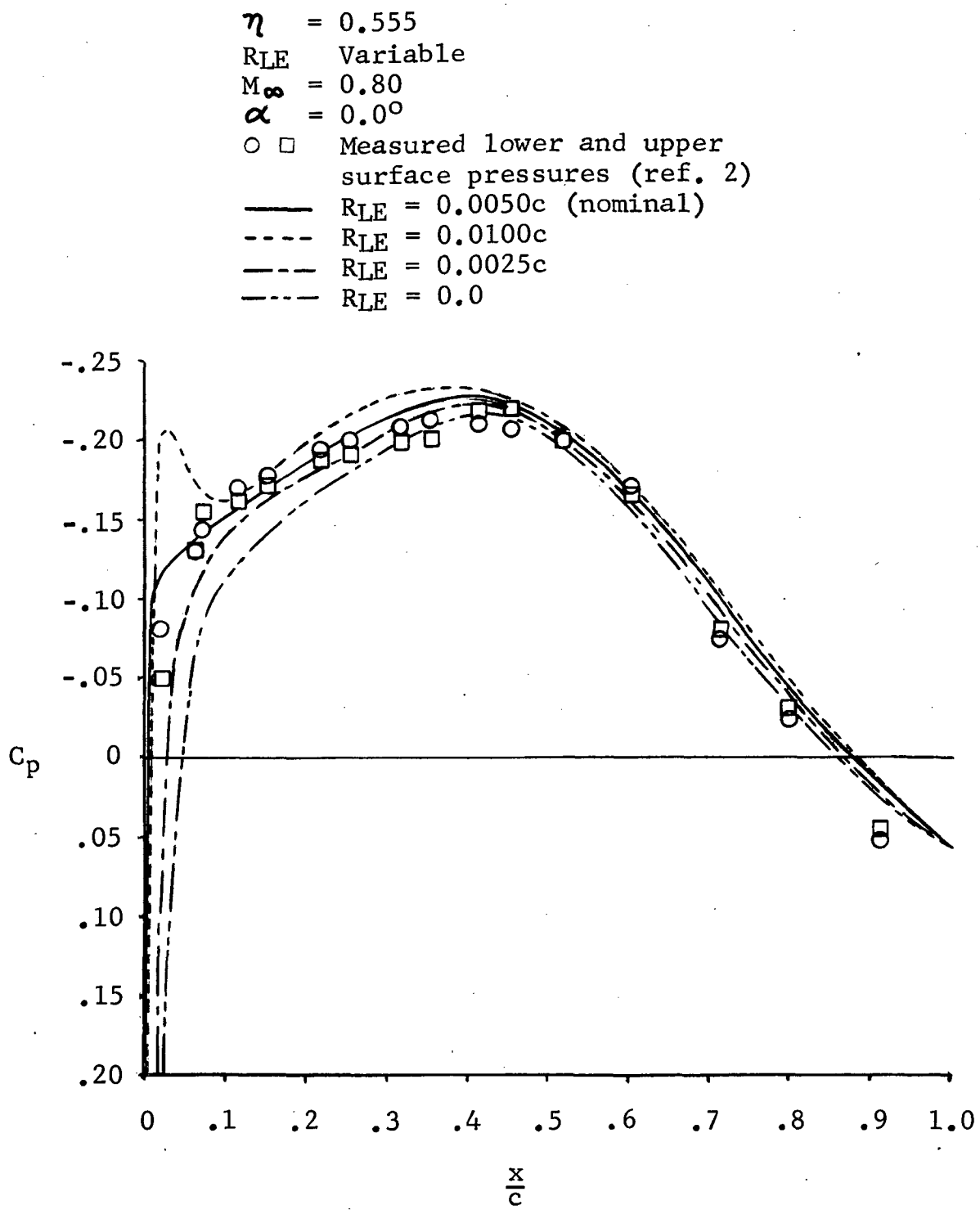

Figure 5.- Effect of R_{LE} on solutions obtained with the experimental M_ℓ distributions.

A study was conducted on the application of leading and trailing edge doublets to a non-lifting case in order to determine the feasibility of the edge singularity method. The problem solved was identical to that shown in Figure 5 for R_{LE} = 0.005c (solid line), with the exception that leading and trailing edge doublets were used in place of the diaphragms shown in Figure 1. Two configurations were considered as shown in Figure 6. The second configuration differed from the first only in the placing of the control points for satisfying the trailing edge Kutta condition as shown in the figure. Since the upper and lower surface flow fields were symmetric, zero downwash was the only condition that had to be satisfied at the leading and trailing edge external control points. Figure 7 shows the results for configurations 1 and 2 as compared with the diaphragm solution from Figure 5. The most interesting effect is the drastic change of the leading edge pressures as a result of changing only the trailing edge control point location. The use of the leading edge doublet seems to degrade the improvement gained with the leading edge line source. Finally, the most obvious change is at the trailing edge where configuration 1 yields a solution that is similar to that obtained without the diaphragm (dashed line, Figure 2). Configuration 2 over corrects the problem and further degrades the leading edge pressures.

The use of line doublets to replace the diaphragms has the advantage of simplicity, however, it does not appear to be adequate. Since the doublets are being used to account for flow discontinuities at the edges, it is obvious that the solution cannot be rigorous. Logarithmic singular type pressure functions would provide the correct characteristics in the edge regions but they would greatly complicate the method.

Modified Diaphragm Method

The diaphragm method discussed above had the disadvantage of not being able to easily treat regions near the leading edge on blunt nose airfoils. The edge singularity method had the disadvantage of requiring the use of sophisticated singularities rather than simple line doublets to meet the edge boundary conditions. The combination of the leading edge line source with the diaphragm method which was used to demonstrate the effect of varying R_{LE} (Figure 5), however, appears to be the logical approach. This modified diaphragm method maximizes the advantages and minimizes the disadvantages of both. Although the

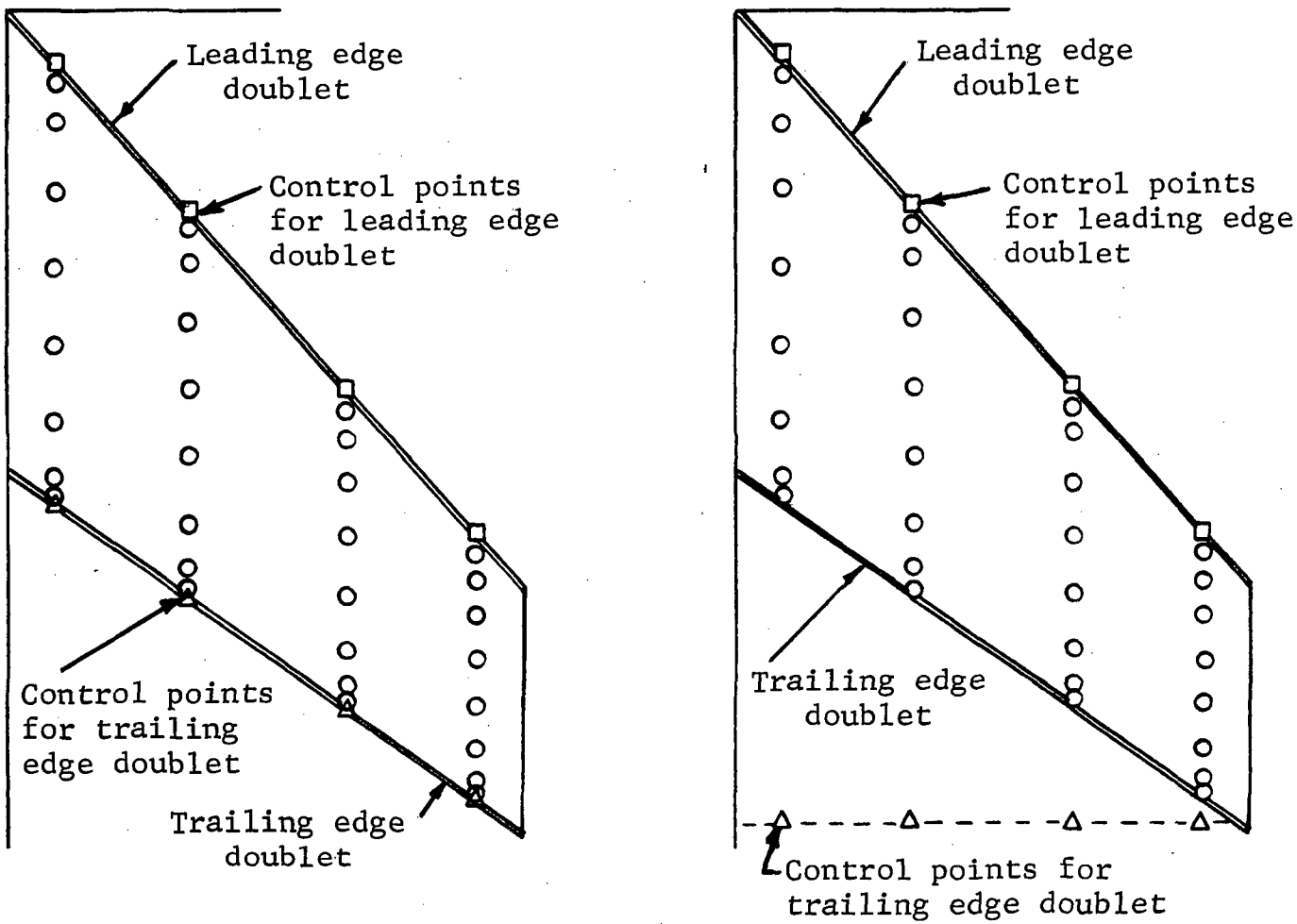

Figure 6.- Variations in the edge singularity configuration for non-lifting cases

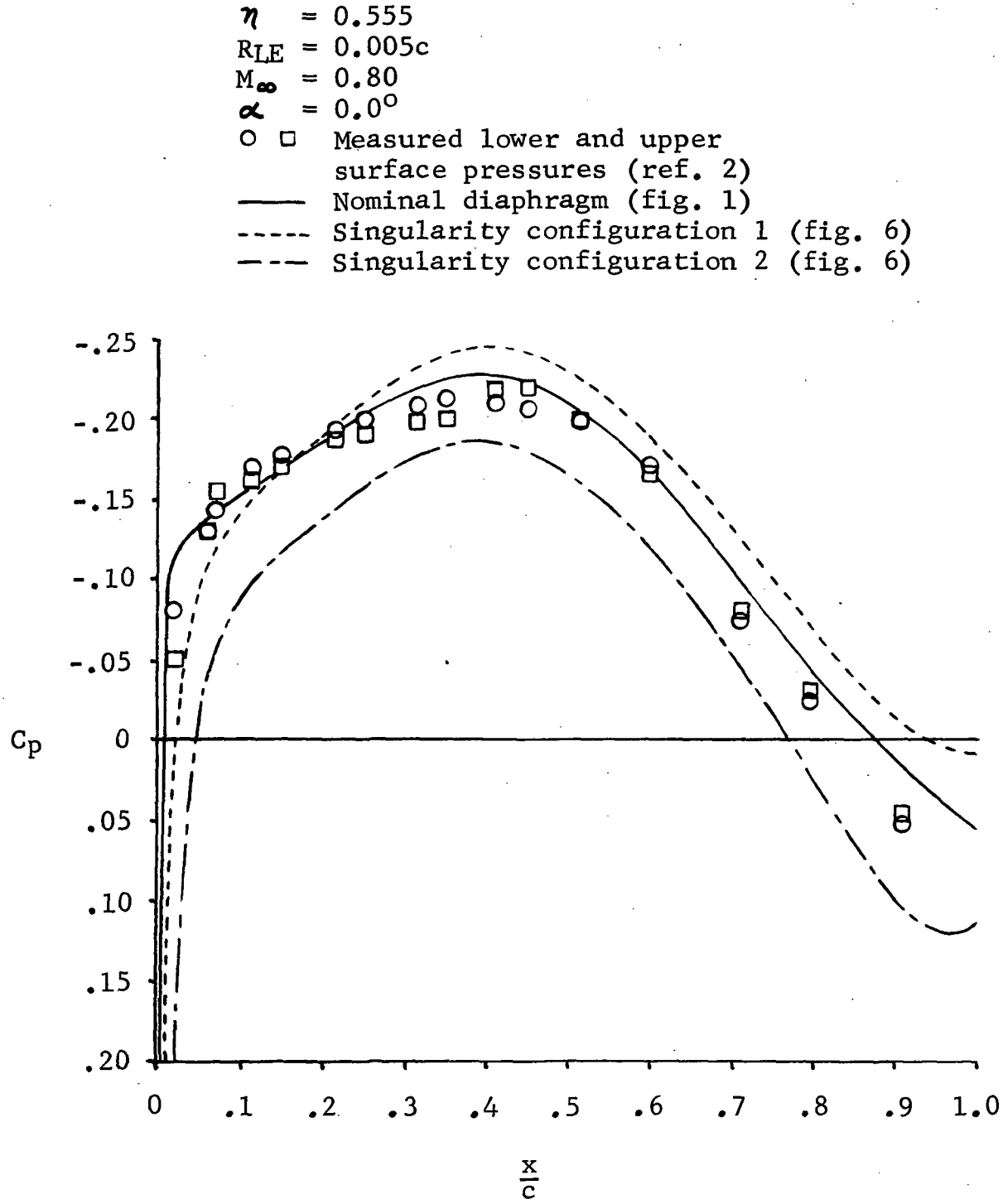

Figure 7.- Comparison of edge singularity and diaphragm solutions with the experimental M_ℓ distributions.

diaphragm still exists in this method, the total number of additional unknown quantities as compared to the edge singularity method is nominally two in the chordwise direction and one in the spanwise direction (if a tip diaphragm is used). This is a small price to pay for keeping the basic simplicity of the diaphragm method.

The equation for the non-lifting modified diaphragm method is the same as equation 1 with exception of the right hand side.

$$\left[\begin{array}{c|c} A_{DD} & A_{DW} \\ \hline A_{WD} & A_{WW} \end{array}\right] \left\{\begin{array}{c} a_D \\ \hline a_W \end{array}\right\} = \left\{\begin{array}{c} 0 \\ \hline \frac{1}{2} w_w' \end{array}\right\} \tag{7}$$

where

$$w_w' = \frac{\partial z_L}{\partial x} - \tan\left(\theta_S + \theta_v'\right) \tag{8}$$

The angle θ_S is the angle of the z_S surface given in the appendix

$$\theta_S = \tan^{-1}\left(\frac{\partial z_L}{\partial x}\right)_x$$

The angle θ_v' is the flow angle induced by the residual wash, $\bar{w}$, normal to the z_S surface and is defined as

$$\theta_v' = \tan^{-1}\left(\frac{\bar{w}}{\bar{u}_L}\right) \tag{9}$$

where

$$\bar{u}_L = \frac{M_L U_\infty}{M_\infty}\left[\frac{2 + (\gamma-1) M_\infty^2}{2 + (\gamma-1) M_L^2}\right]^{1/2}$$

It should be noted that θ_v' is based on the total local tangential velocity, $\bar{u}_L$, rather than the value $\bar{u}$ which is induced only by the leading edge line source and the free stream flow (see equations A20).

The equation for the lifting modified diaphragm method is likewise similar to equation 5 with exception of the right hand side:

$$\begin{bmatrix} 2A_{DD} & A^{U}_{DW} & A^{L}_{DW} \\ A^{U}_{WD} & A^{U}_{WW} & 0 \\ A^{L}_{WD} & 0 & A^{L}_{WW} \end{bmatrix} \begin{Bmatrix} a_D \\ a^{U}_{W} \\ a^{L}_{W} \end{Bmatrix} = \frac{1}{2} \begin{Bmatrix} 0 \\ w'_{W_U} \\ w'_{W_L} \end{Bmatrix} \tag{10}$$

where

$$w'_{W_U} = \frac{\partial z_U}{\partial x} - \tan\left(\theta_s + \theta'_v\right)_U \tag{11a}$$

$$w'_{W_L} = \frac{\partial z_L}{\partial x} - \tan\left(\theta_s + \theta'_v\right)_L \tag{11b}$$

Although θ_s is the same on the upper and lower surfaces, θ'_v will be different as a result of the different velocity fields.

The next section will be devoted to verification of the modified diaphragm method as an economical means for obtaining converged solutions for finite thickness wings in the high subsonic flow regime.

VERIFICATION OF THE MODIFIED DIAPHRAGM METHOD

Studies performed with the final method will be summarized in this section for both non-lifting and lifting cases in sub-critical flow. Convergence of the method will be demonstrated and the results compared with a solution obtained with M_ℓ distributions taken from experimental data. The effect of adding a simple boundary layer model will be shown. Also, the importance of accurately determining the surface slopes as well as using adequate trailing edge diaphragms will be demonstrated. In all solutions obtained, R_{LE} = 0.005c was used.

Convergence of the Solution

Shown in Figure 8 are three iterations for a solution to the non-lifting problem which has been the subject of the previous section. The case was for $\alpha = 0^{\circ}$ and $M_{\infty} = 0.80$ in which the diaphragm used is shown in Figure 1. The first iteration was obtained with a uniform M_{ℓ} distribution on both the wing and diaphragms, equal to $M_{\infty} = 0.80$. The M_{ℓ} distribution calculated from the uniform flow solution was used as the input for the second iteration. The third iteration was obtained with a M_{ℓ} distribution produced by the second solution. The second and third iterations shown in Figure 8 clearly demonstrate that the solution has converged.

Figure 9 shows a comparison between the third iteration solution and that obtained with the M_{ℓ} distribution determined from experimental data. The differences in M_{ℓ} used, as indicated by the theoretical and experimental C_p distributions, are much greater than the calculated values of C_p. Hence, it is concluded that something may be lacking in either the slope distributions used or the diaphragm representation.

Convergence is shown in Figure 10 for the same wing in the same flow with $\alpha = 2^{\circ}$. The first iteration was obtained with the M_{ℓ} distribution calculated on the third iteration above for $\alpha = 0^{\circ}$. The second and third iterations in Figure 10 were obtained in the same manner previously described. In this case, the differences noted above are more emphasized in the comparison of converged theory and experiment.

An attempt was made to demonstrate convergence for the same wing at $M_{\infty} = 0.96$, $\alpha = 0^{\circ}$ where the flow became locally supersonic. Problems were encountered that produced erratic results for iterations which had supersonic flow. The nature of the results indicated that a possible error existed in the steady flow portion of the computer program used in this study. The same program, however, was successfully used to solve steady flow problems with mixed subsonic and supersonic flow and imbedded shocks (ref. 1). These cases were for rectangular wings, which did not require use of certain parts of the program. The suspected parts were examined for possible errors, however, nothing was found that could cause what was observed. Thus for purposes of this study, the mixed flow case was abandoned.

η = 0.555
R_{LE} = 0.005c
M_∞ = 0.80
α = 0.0°
○ □ Measured lower and upper surface pressures (ref. 2)
—— First iteration ($M_\ell = M_\infty$ = uniform)
---- Second iteration (M_ℓ from first iteration)
—-— Third iteration (M_ℓ from second iteration)

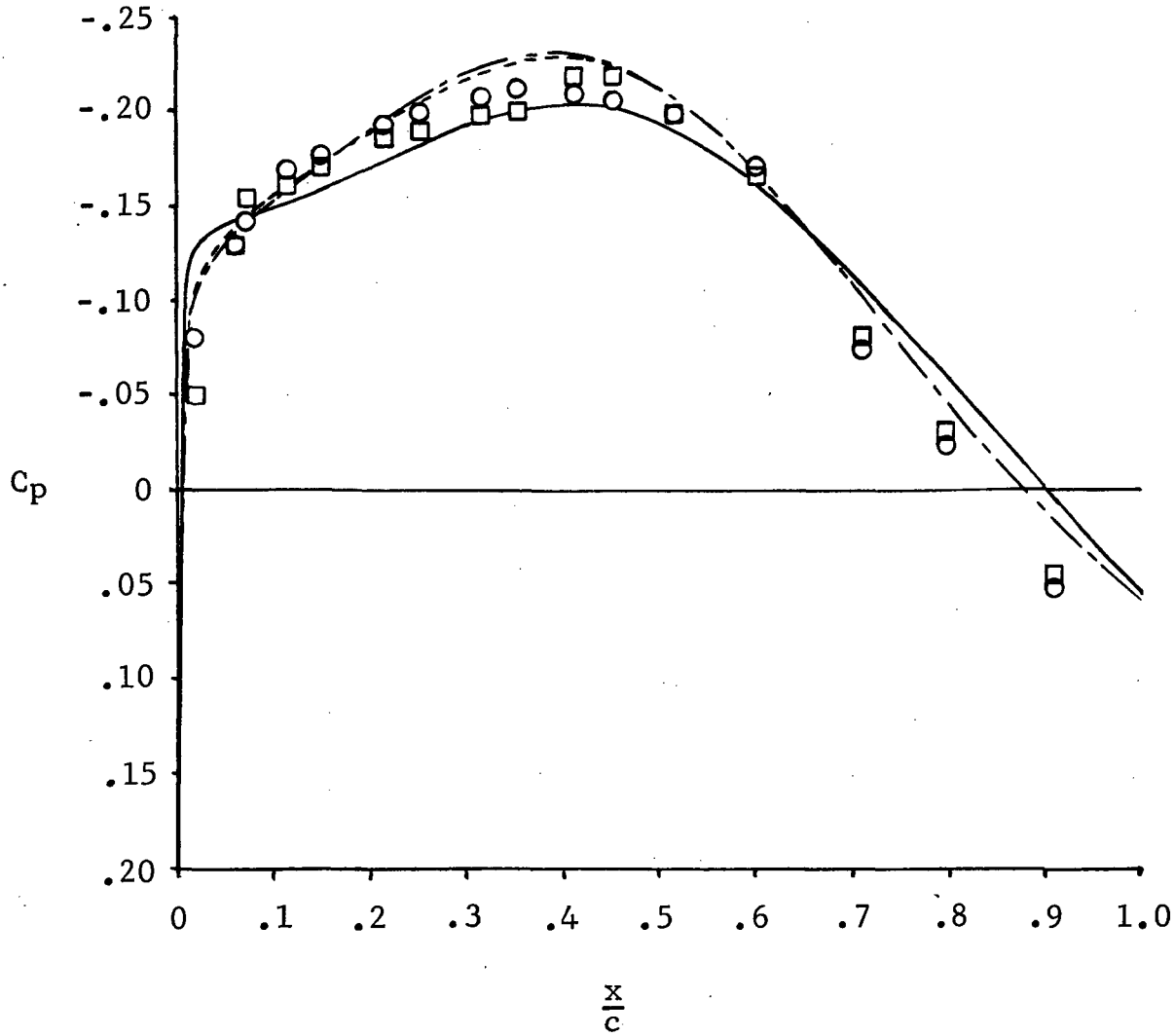

Figure 8.- Convergence of the theoretical solution for α =0°.

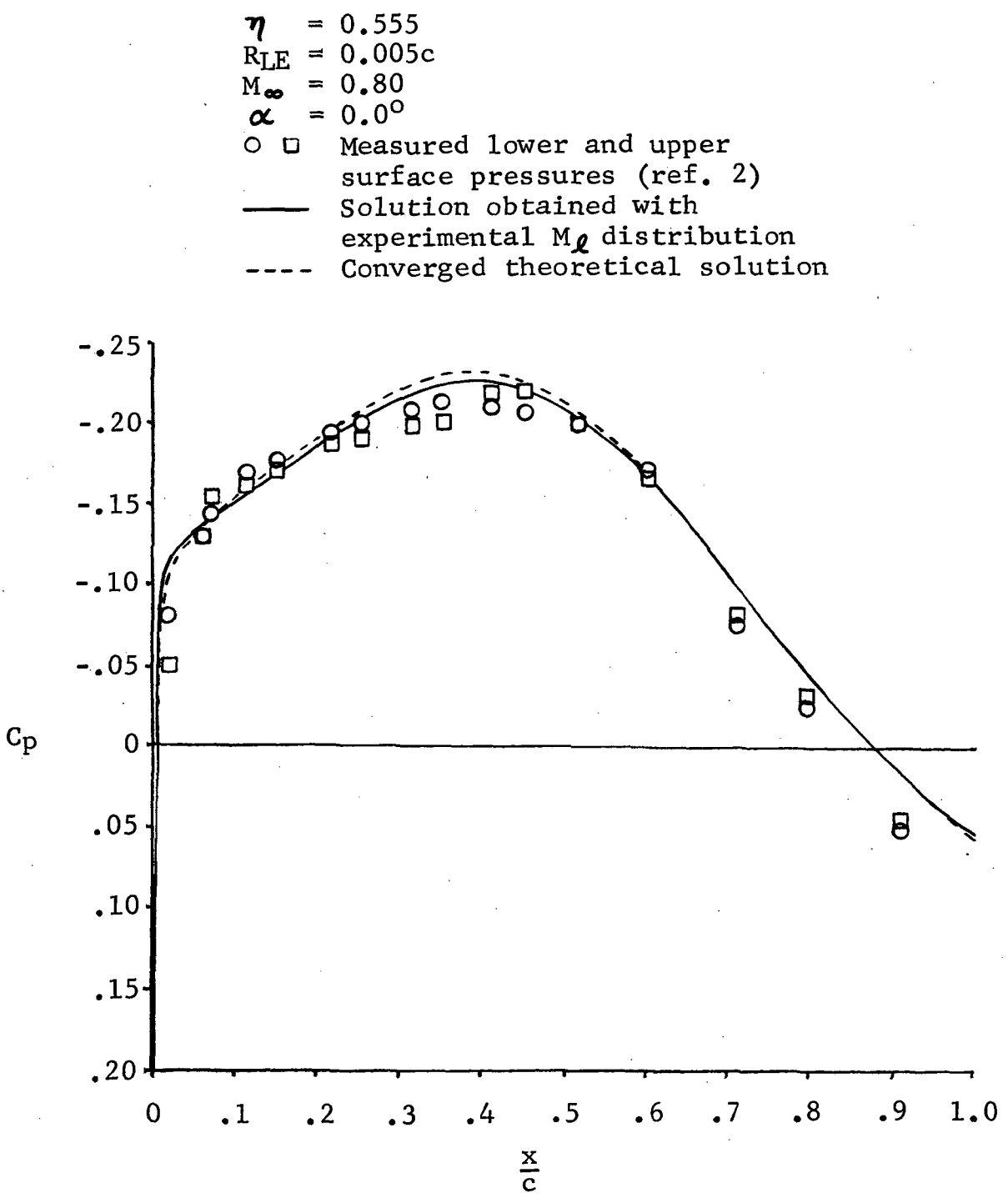

Figure 9.- Comparison of solutions obtained with experimental M_ℓ distribution and theory for $\alpha = 0^\circ$.

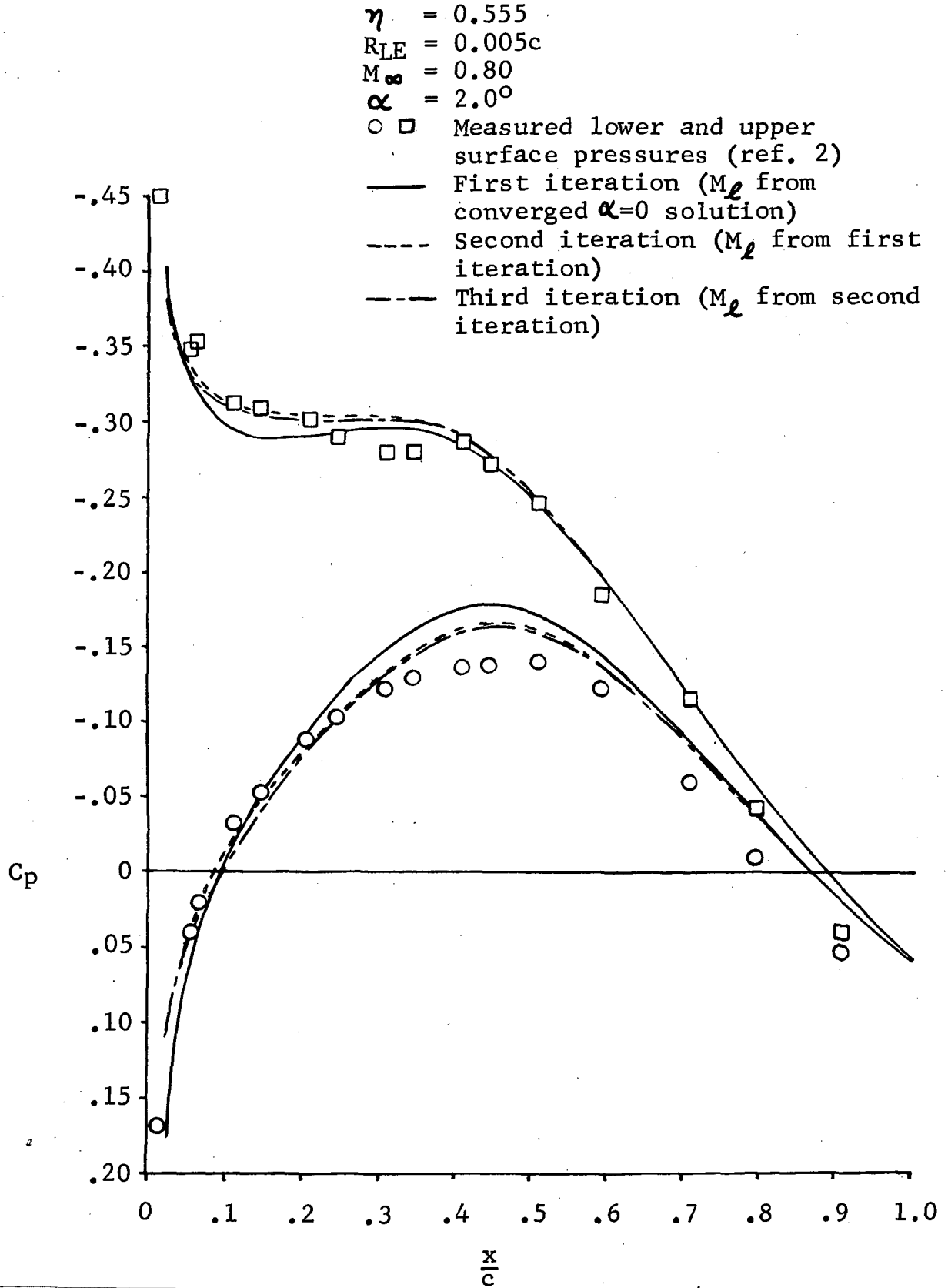

Figure 10.- Convergence of the theoretical solution for $\alpha = 2^{\circ}$.

Possible Sources of Error

Several effects were examined as possible sources of error in the theoretical solution. Because of the closeness in agreement between solutions obtained with experimental values of M_ℓ and theoretical values, the experimental distribution was used in these studies. In doing so, the calculated solution should agree with experiment if all of the errors were removed.

Boundary layer effects.- Shown in Figure 11 is the effect of including a simple ramp type boundary layer displacement thickness, δ^*. The slope increment was determined from the value of δ^* at the trailing edge obtained from the turbulent boundary layer formula (ref. 3)

$$\delta^* = \frac{0.37x}{8}\left(\frac{U_\infty x}{\nu}\right)^{-1/5}$$

The slope was assumed constant at $\partial\delta^*/\partial x \approx 0.022$, hence, the results in Figure 11 only indicate order of magnitude and general characteristics of the boundary layer effect. This model also will not account for local separation. Since the effects of δ^* as shown in this illustration do not enhance the agreement between calculated and measured C_p's, it is felt that this is not the major problem.

Effect of errors in measuring surface thickness slopes.- The surface thickness slopes were measured again more accurately and some differences were found as indicated in Table 1.

TABLE 1. SURFACE THICKNESS SLOPES FOR AN NACA 64A010 AIRFOIL AT 45° SWEEP (REF. 2)

$\frac{x}{c}$	$\partial z_t/\partial x$ Original	$\partial z_t/\partial x$ Remeasured
0.0338	0.100	0.100
0.1305	0.046	0.046
0.2772	0.022	0.019
0.4539	-0.007	-0.005
0.6369	-0.032	-0.032
0.8013	-0.042	-0.042
0.9251	-0.043	-0.043
0.9915	-0.044	-0.043

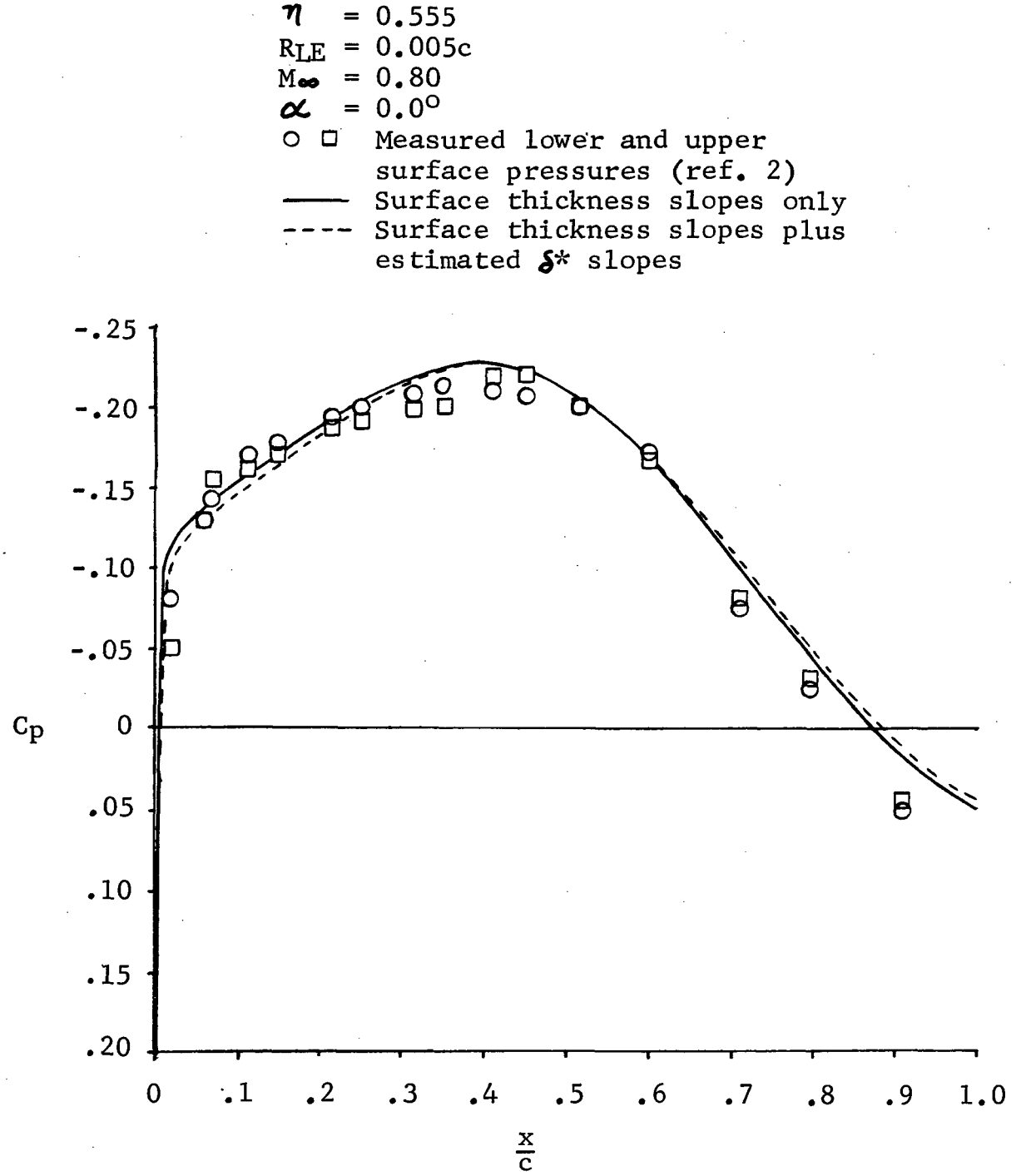

Figure 11.- Effect of estimated boundary layer displacement thickness, δ^*, on solutions obtained with experimental M_ℓ distribution.

Although the differences were small, the resulting calculated C_p's shown in Figure 12 indicate that their impact is significant. With exception of near the trailing edge, the calculated C_p's now show a remarkable agreement with measured values. Thus, it is concluded that correct measurement of surface thickness slopes is a very critical necessity.

Effect of the trailing edge diaphragm.- As was discussed in the evaluation of the edge singularity method, how the trailing edge is treated has considerable influence in the total solution. Figure 13 shows the configuration with a doubled trailing edge diaphragm with three chordwise functions. The new diaphragm had the same chord and aspect ratio as well as number of pressure functions as the leading edge diaphragm. The result of using the larger diaphragm is shown in Figure 14. Although the change was not large, the solution was improved in the trailing edge region. It is concluded that the use of diaphragms needs further study in order to determine the relative importance of the parameters involved.

Final Predictions for $\alpha=0^\circ$ and $\alpha=2^\circ$

On the basis of what was learned in the above studies, final solutions for $\alpha=0^\circ$ and $\alpha=2^\circ$ were assembled with: M_ℓ distributions obtained from the third iteration; enlarged trailing edge diaphragm; and remeasured surface thickness slopes.

The results at $M_\infty=0.8$ and $\alpha=0^\circ$ are shown in Figure 15 for three span stations. A comparison is made between the modified diaphragm method (final solution), uniform flow over a single surface, and experiment. As can be seen, the new method is far superior to the uniform flow solution with a single surface. The computer costs on a CDC 6600 are shown in the following table.

	CP sec
Single Wing, Uniform Flow	13.5
1st Iteration	23.2
2nd Iteration	23.2
3rd Iteration	23.2
4th Iteration (expanded diaphragm)	24.5
Iteration Solution Total	94.1

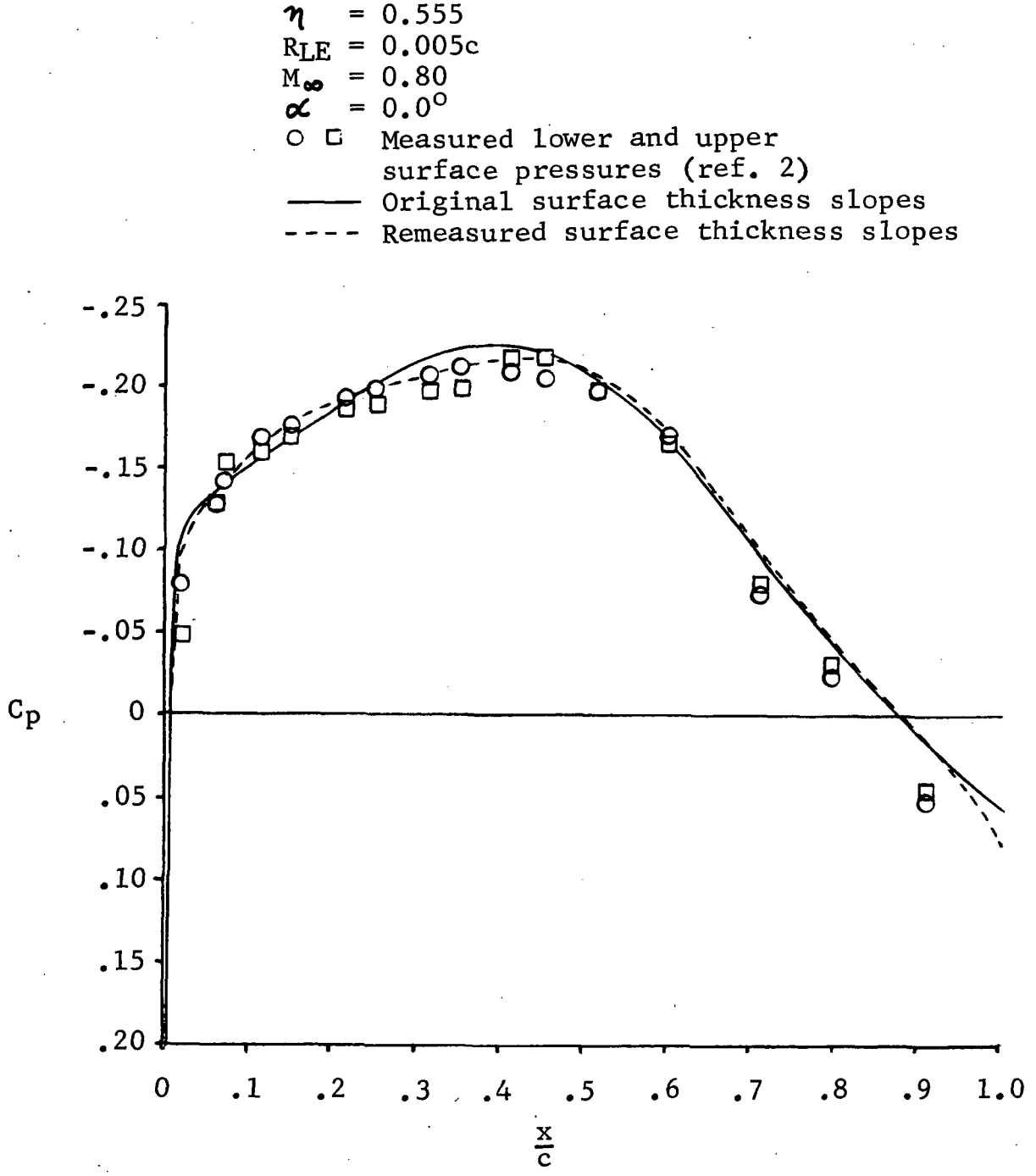

Figure 12.- Effect of the accuracy of the measured surface thickness slopes on solutions obtained with experimental M_ℓ distributions.

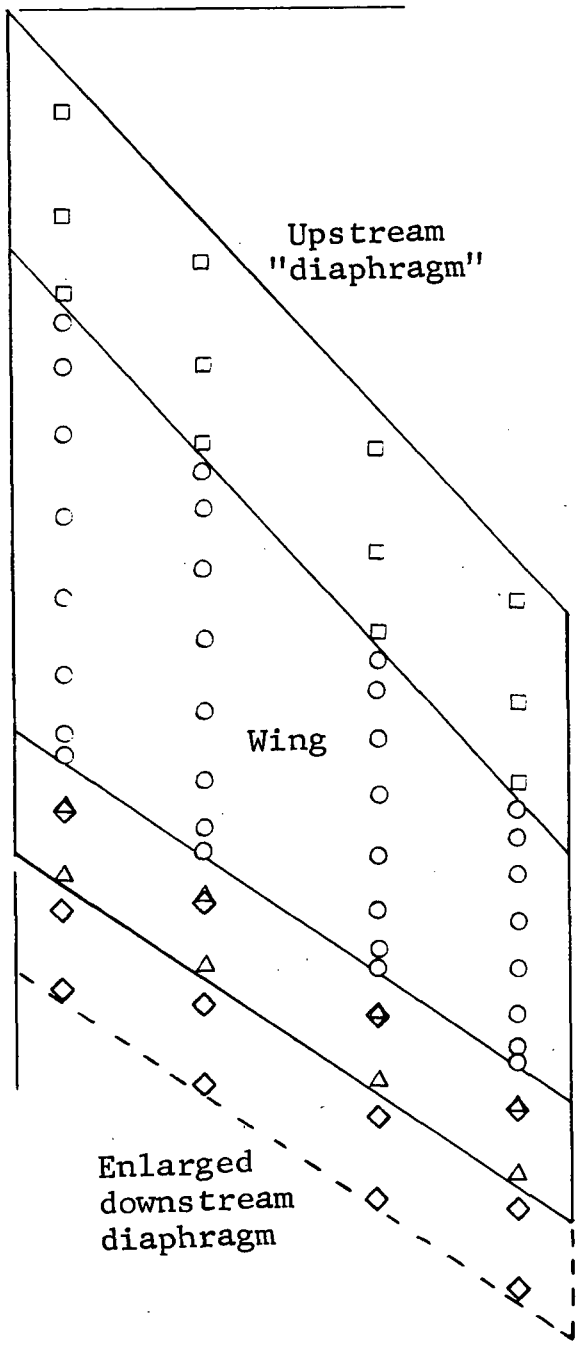

Figure 13.- Geometry and downwash point array for a diaphragm solution for the wing of ref. 2 with enlarged trailing edge diaphragm.

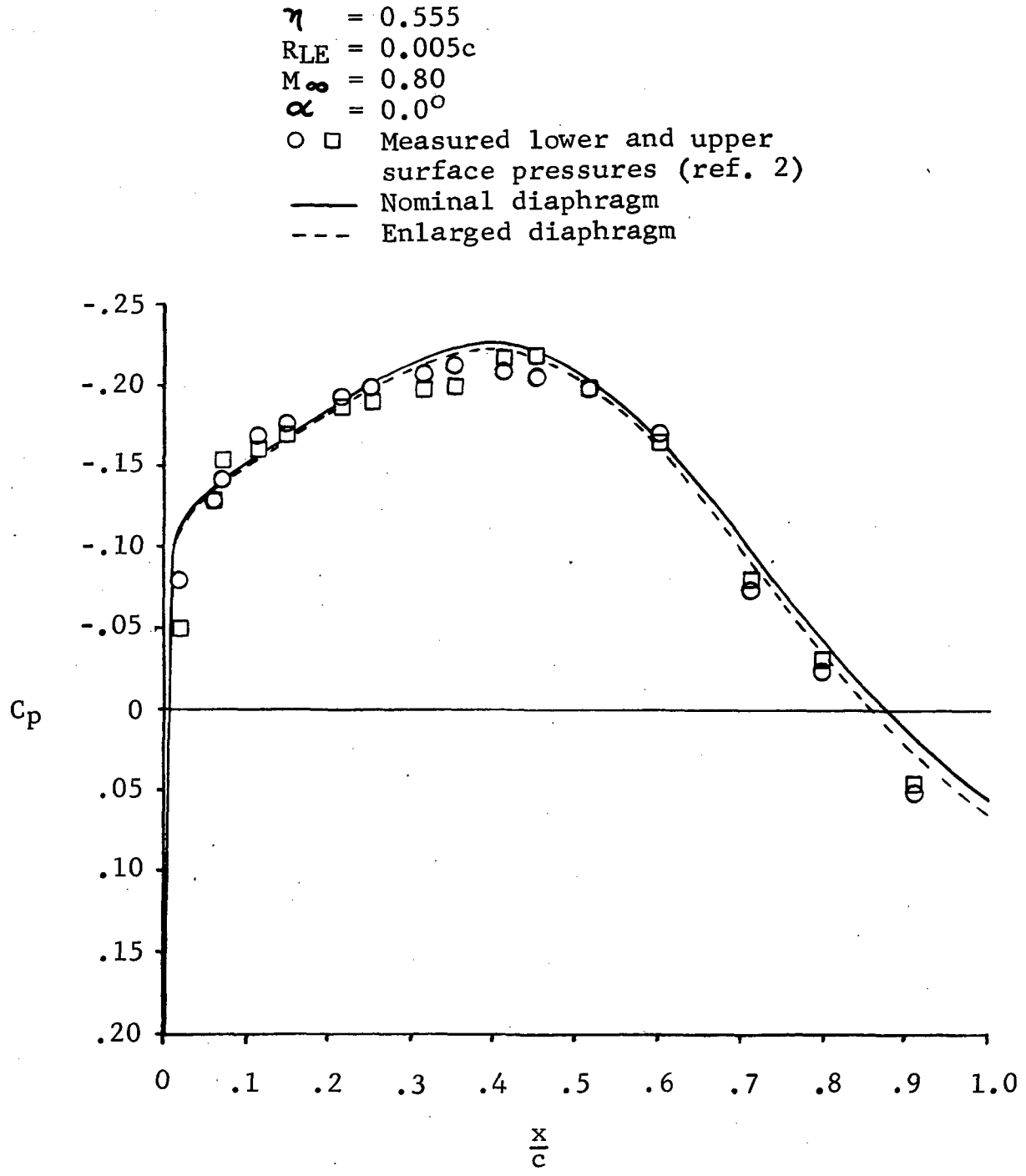

Figure 14.- Effect of trailing edge diaphragm size on solutions obtained with experimental M_ℓ distributions

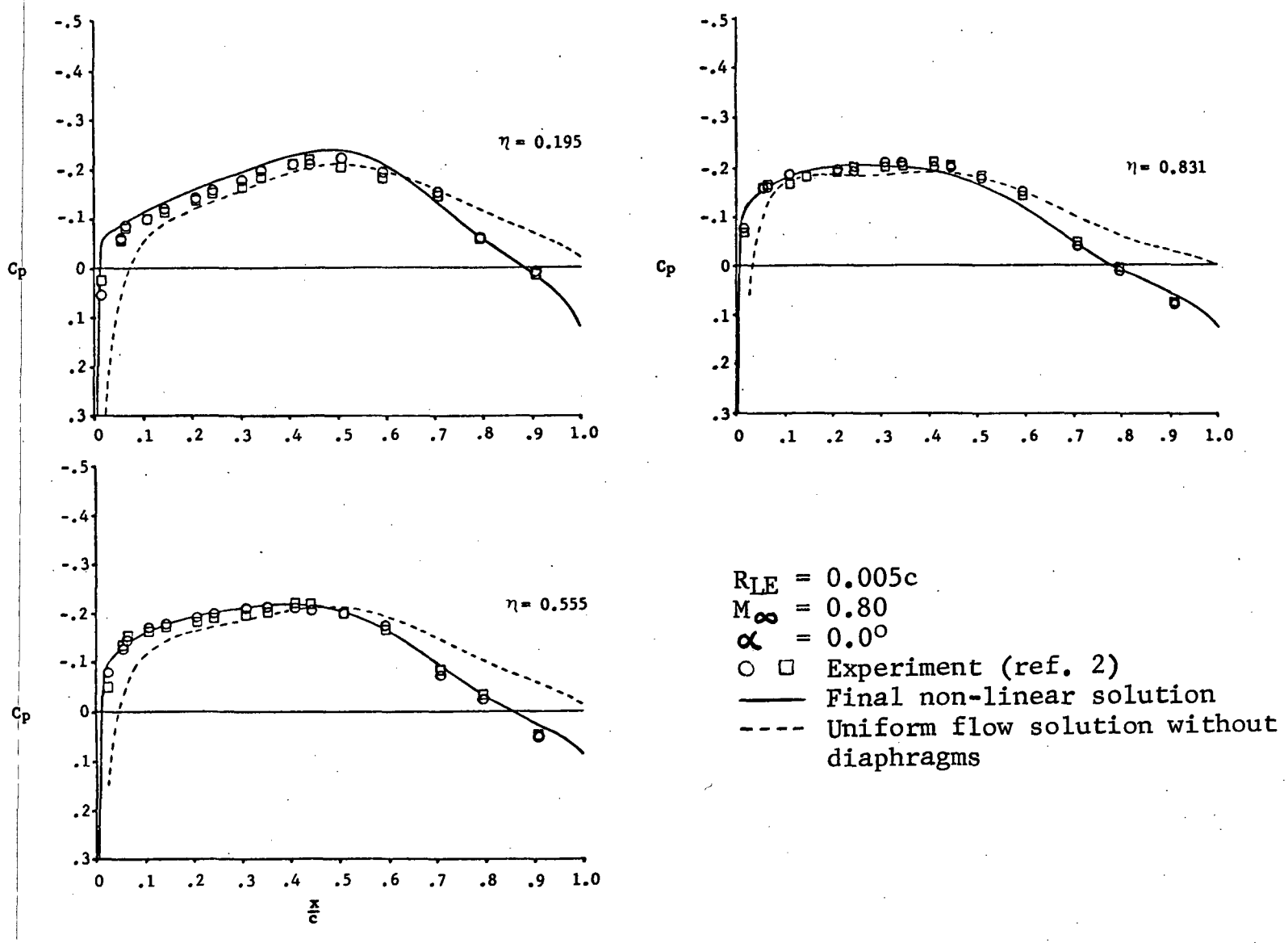

Figure 15.- Final non-linear transonic flow solution for the wing of ref. 2 at $\alpha = 0^\circ$ and $M_\infty = 0.80$

Although the total cost of the iterated solution is not large, it could be reduced significantly by automating the procedure. Also, if the third iteration were made with the expanded diaphragm, the fourth iteration would not have been necessary.

The over-prediction at the inboard span station in Figure 15 is felt to be due to the effect of wind tunnel wall boundary layer. Since the model was a semi-span model mounted on the wall without any boundary layer removal, the effect could be significant. It was stated in ref. 2 that the estimated displacement thickness was about 0.5 in. which should have a negligible effect on a model with a semi-span of 46.7 in. The pressure isobars shown in ref. 2 at $\alpha=2^{o}$, however, did not verify this assumption since they had a tendency to become parallel to the wall near the leading edge.

The mid-span station shows excellent agreement with experiment since it was the least influenced by possible wall boundary layer effects and absence of a tip diaphragm. The outboard station also shows excellent agreement which was apparently due to the fact that the leading edge diaphragm tip vortex was in opposition to that shed by the wing. Thus, it was felt that large tip diaphragms may not be necessary.

A comparison is made in Figure 16 for $\alpha=2^{o}$ between mid-span pressures calculated with the original and the remeasured thickness slopes. Both solutions were obtained with the M_{ℓ} distribution from the third iteration and the large trailing edge diaphragm. The effect of the correction at $\alpha=2^{o}$ is about the same as that seen at $\alpha=0^{o}$ in Figure 12.

Figure 17 shows the final results at three span stations for $M_{\infty}=0.8$ and $\alpha=2^{o}$. The same comparison is made again to show the superiority of the modified diaphragm method. The differences between the theories are even more striking at $\alpha=2^{o}$. The computer costs on a CDC 6600 are given in the following table.

	CP sec
Single Wing, Uniform Flow	13.5
1st Iteration	41.3
2nd Iteration	41.3
3rd Iteration	41.3
4th Iteration (expanded diaphragm)	43.1
Iteration Solution Total	167.0

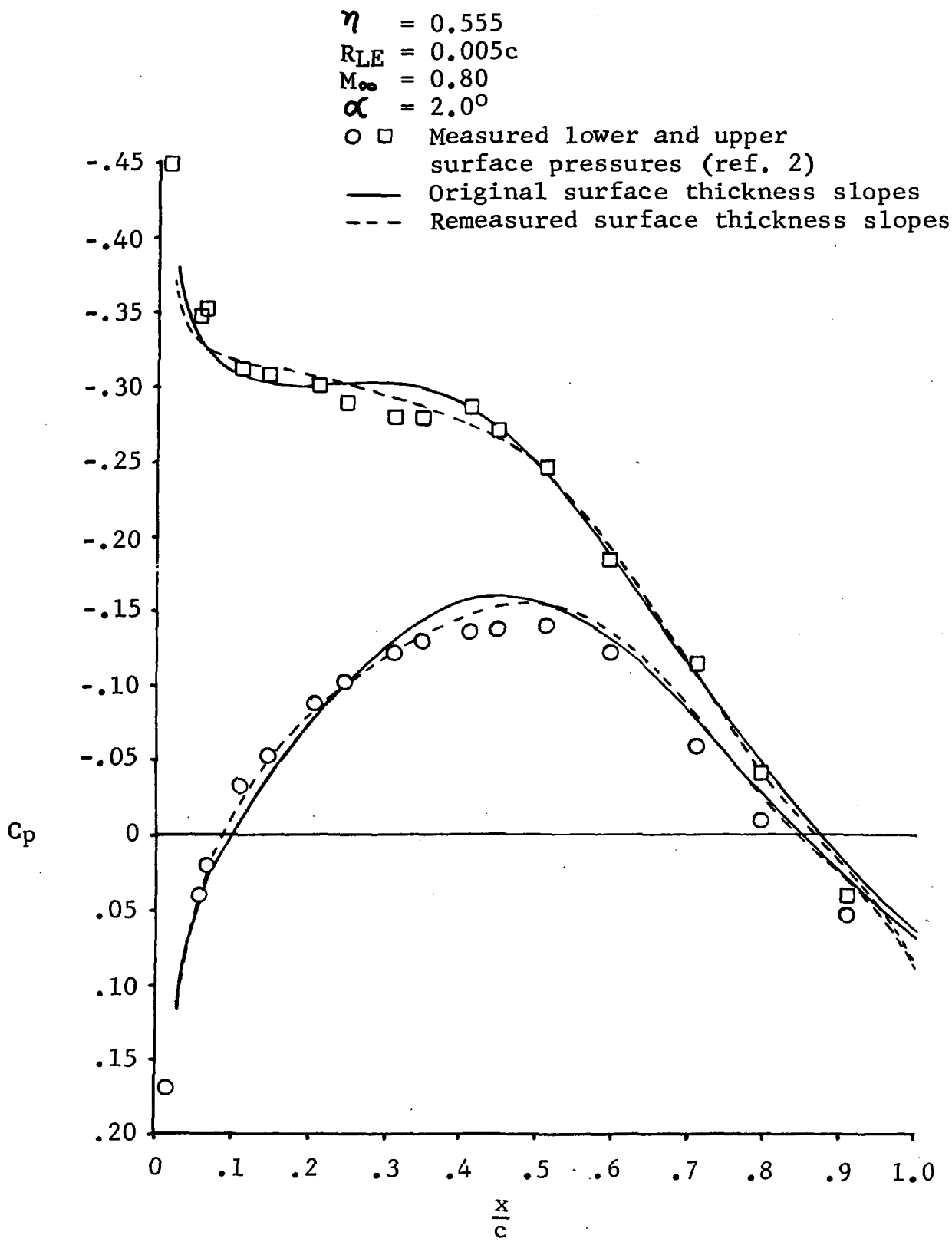

Figure 16.- Effect of the accuracy of the measured surface thickness slopes on the non-linear transonic flow solution for the wing of ref. 2 at $\alpha = 2^{\circ}$ and $M_{\infty} = 0.80$

As with the $\alpha=0^{\circ}$ case, if the third iteration were made with the expanded diaphragm the fourth would not be needed.

The discussion on disagreement between theory and experiment given for $\alpha=0^{\circ}$ is applicable to $\alpha=2^{\circ}$. It is interesting to note that the agreement improved slightly for the mid-span station whereas it was degraded forward and improved aft along the inboard station. The tip station results showed a degradation on the upper surface and an improvement on the lower surface. Hence, the tip diaphragm may become more important with increasing angle of attack or lift.

CONSIDERATIONS FOR UNSTEADY FLOW CALCULATIONS

An obvious question that arises when considering the calculation of unsteady flow perturbations on the upper and lower surfaces is whether or not the solutions can be considered as independent in the case of non-symmetric flow fields. Or, in terms of the modified diaphragm method, would it be necessary to obtain a complete upper and lower surface solution with diaphragms for unsteady perturbations or would simple uncoupled single wing solutions for each side suffice. The answer to this question cannot be realized without obtaining both solutions to the same problem and comparing the results. However, some insight can be gained on the basis of what has already been done.

A comparison of the results for $\alpha=0^{\circ}$ and $\alpha=2^{\circ}$ in Figures 15 and 17 shows that the trailing edge pressure coefficient changes very little at each span station for a change in α. Likewise, the pressure distribution in the diaphragm changes very little. Thus, for small changes in lift, the presence of the diaphragm is of second order importance in the case of subcritical flow at low angles of attack.

Magnus and Yoshihara (ref. 4) have calculated non-linear unsteady pressures on a two dimensional airfoil oscillating in mixed transonic flow with an embedded shock. For a wide range of reduced frequencies, k=0 to k=5, their results also show that the trailing edge pressure coefficient remains unchanged at about the steady state value throughout the cycle of oscillation. The flows are vastly different on the upper and lower surfaces which gives further justification for assuming that the flows may be treated independently.

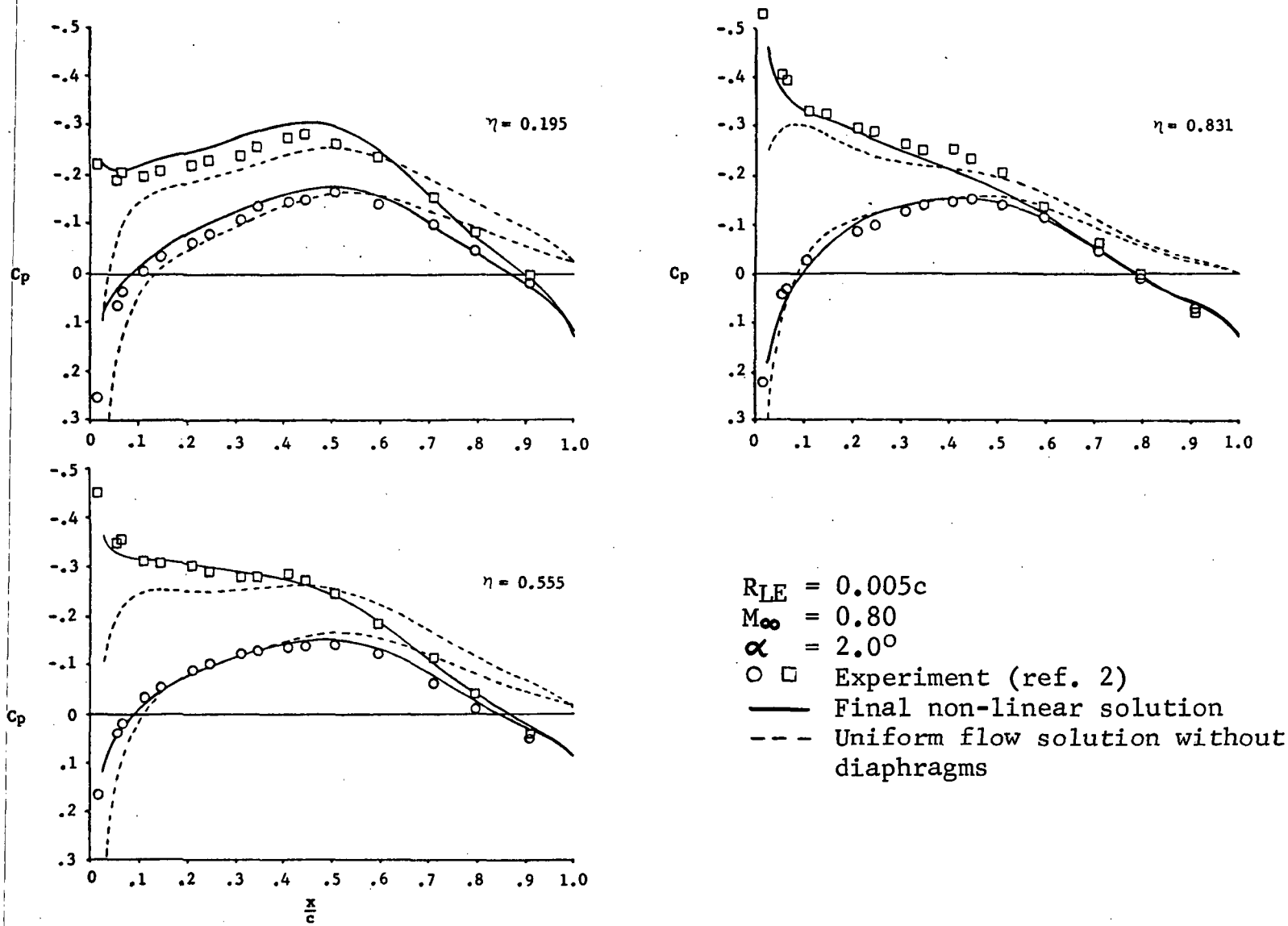

Figure 17.- Final non-linear transonic flow solution for the wing of ref. 2 at $\alpha = 2^{\circ}$ and $M_{\infty} = 0.80$

Thus, it is felt that good results can be obtained with decoupled solutions as long as the correct upper and lower surfaces Mach number distributions are used. Coupled solutions are needed, however, to determine what increase in accuracy is gained with what increase in cost. Also, since larger matrices will be required which are complex, computer core storage availability becomes a limiting factor for the coupled solutions.

CONCLUSIONS AND RECOMMENDATIONS

A study has been conducted in order to determine the feasibility of calculating non-linear steady flow solutions at transonic speeds with the non-uniform flow linear theory aerodynamic method of ref. 1. Two approaches were studied which included a diaphragm method and an edge singularity method. The objective of both approaches was to couple together the linear theory aerodynamic solutions for the upper and lower surfaces of a wing with finite thickness. The investigation of the two methods led to the development of the modified diaphragm method which was a combination of the two original approaches.

The modified diaphragm method was demonstrated to be a powerful tool for obtaining high subsonic aerodynamic solutions for wings with blunt nose airfoils. A leading edge line source was used to remove the stagnation flow characteristics from the solution which left only a thin wing problem to solve on the upper and lower surfaces. The non-uniform aerodynamic method of ref. 1 was then used to solve the thin wing problems where the upper and lower surface solutions were coupled only through external diaphragm regions surrounding the wing. Free surface boundary conditions were satisfied on the diaphragms.

The method was found to converge rapidly to very accurate solutions when used in an iteration scheme in high subsonic flow which was subcritical. The case involved a swept tapered wing with a symmetric airfoil in $M_\infty=0.8$ flow at $\alpha=0^\circ$ and 2°. Starting with a uniform flow solution, a converged non-uniform flow solution was obtained in two more iterations. Then starting with a solution obtained with the converged flow field for $\alpha=0^\circ$, a converged solution was found for $\alpha=2^\circ$ in two more iterations.

The leading edge line source and the trailing edge diaphragm had the greatest influence on the aerodynamic solutions in the leading and trailing edge regions, respectively. The accuracy of the surface thickness slopes was found to be a very critical item in the total solution. The result of including an estimated boundary layer displacement thickness was inconclusive but the effect was found to be of second order importance.

In an attempt to demonstrate convergence on the same wing at $M_\infty = 0.96$, $\alpha = 0^\circ$, some erratic results were encountered in iterations which had supersonic flow. The nature of the results indicated that an error might exist in the steady flow portion of the aerodynamic computer program. The program was examined for possible errors, however, nothing was found that could cause what was observed. Thus, for purposes of this study, the mixed flow case was abandoned.

The effect of coupled upper and lower surface solutions for unsteady flow was considered. It was felt that good results can be obtained with decoupled solutions as long as the correct upper and lower surface Mach number distributions were used. Coupled solutions are needed, however, in order to access the differences that are introduced, if any, by neglecting the effect.

In conclusion it is recommended that the aerodynamic computer program of ref. 1 be modified so as to have the capability to calculate non-linear transonic steady mean solutions by the use of the modified diaphragm method. The following tasks are recommended as a means of achieving this capability:

1. Debug the section of the program responsible for the error encountered. (The problem is felt to be associated with coordinate transformations in the steady part of the program which are made for swept surfaces in supersonic flow. Hence, the difficulty was not noted for rectangular wings.)

2. Modify the program to use the more correct form of the downwash-pressure function integral equation as suggested in ref. 1

$$-\frac{U_{xy}}{U_\infty}\frac{\partial z}{\partial x} = \frac{1}{8\pi}\iint \frac{U_{\xi\eta}}{U_{xy}} \Delta C_p(\xi,\eta) K(x-\xi, y-\eta, z-\zeta, M_{xy})\, d\xi\, d\eta$$

where U_{xy} and $U_{\xi\eta}$ are the velocities at the downwash and integration points, respectively, and K( ) is the kernel function.

3. Develop a practical means for achieving highly accurate surface thickness slopes. (As an example, surface thickness and camber coordinates could be input at 20 points along each downwash chord and interpolated with either a local cubic or one dimensional spline to obtain the slopes.)

4. Verify the modified diaphragm method for mixed flow over both swept and rectangular wings.

5. Develop an automated iteration procedure which is terminated by either a convergence criteria or input limits on number of iterations.

6. Investigate the effect of a diaphragm on unsteady aerodynamics.

7. Compare unsteady predictions with experimental results for wings oscillating about both lifting and non-lifting steady flow conditions.

8. Develop an executive capability to assemble the generalized forces for upper and lower surface solutions.

9. Conduct a seminar on the capability and utilization of the final computer program at NASA Langley Research Center.

The resulting computer program should provide the capability to calculate steady mean flow solutions, oscillatory pressure distributions, and generalized forces for wings in mixed transonic flow. The effects of surface thickness, twist and camber distribution, mean angle of attack, aerodynamic interference, and aeroelastic deformation can all be accounted for. The flow fields may be mixed subsonic and supersonic flows with or without embedded shocks. It appears that the capability of the program will be primarily limited only by the imagination and ingenuity of the user.

General Dynamics Corporation
P. O. Box 748
Fort Worth, Texas 76101, February 29, 1976

APPENDIX

LEADING EDGE LINE SOURCE

Calculation of the Velocity Components

Referring to Figure A1, let the strength per unit length, $m(\xi,\eta,\zeta)$, of the line source satisfy the stagnation condition at the leading edge for the velocity component $U_\infty \cos \Lambda_{LE}$. The flow potential $d\phi$ at point x,y,z due to an infinitesimal line segment at ξ,η,ζ is

$$d\phi(x,y,z) = \frac{m(\xi,\eta,\zeta)}{R} \tag{A1}$$

where

$$R^2 = (x-\xi)^2 + \beta^2 r^2$$
$$r^2 = (y-\eta)^2 + (z-\zeta)^2$$
$$\beta^2 = 1 - M^2$$

The total flow potential, ϕ, is thus

$$\phi(x,y,z) = \int_{L_S} \frac{m(\xi,\eta,\zeta)}{\sqrt{(x-\xi)^2 + \beta^2 r^2}}\, dl \tag{A2}$$

where integration is performed along the source line over the length L_S.

Referring to Figure A2, the following geometry transformations are made to the source line coordinate system:

$$x = x_1 + x' \cos \Lambda_{LER} + y' \sin \Lambda_{LER} \tag{A3a}$$

$$y = y_1 + y' \cos \Lambda_{LER} - x' \sin \Lambda_{LER} \tag{A3b}$$

$$\xi = x_1 + \xi' \cos \Lambda_{LER} + \eta' \sin \Lambda_{LER} \tag{A3c}$$

$$\eta = y_1 + \eta' \cos \Lambda_{LER} - \zeta' \sin \Lambda_{LER} \tag{A3d}$$

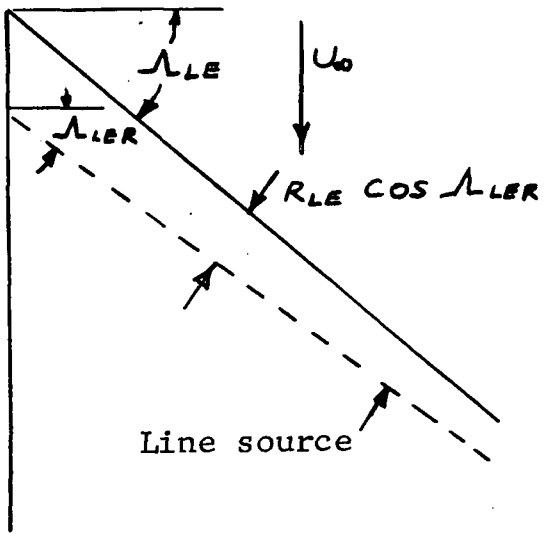

Figure A1.- Leading edge line source configuration

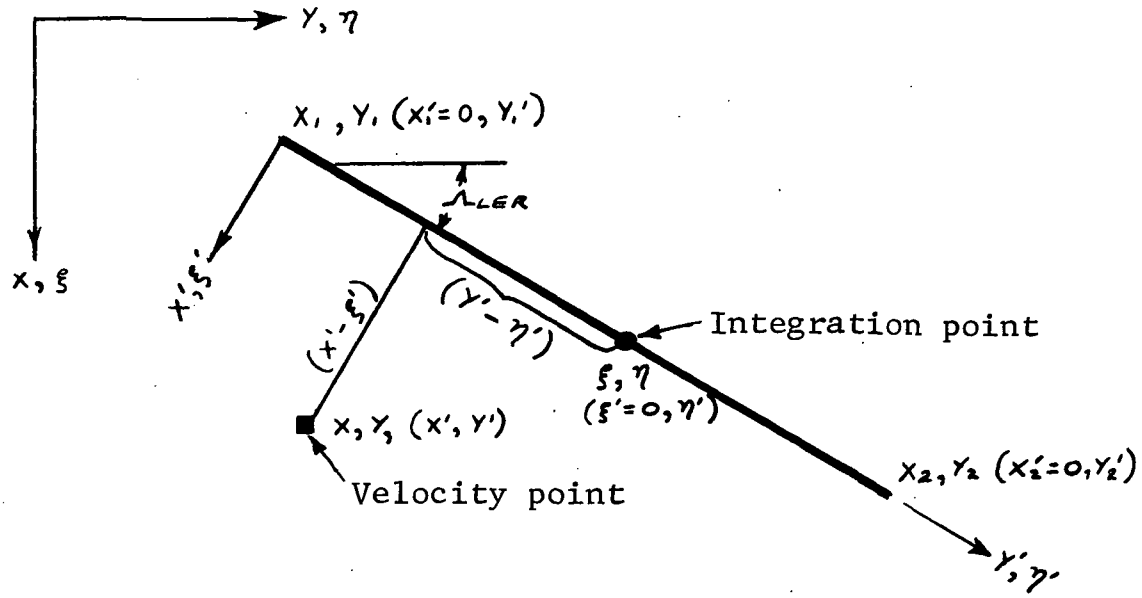

Figure A2.- Coordinate systems for a leading edge line source

Since $\xi' = 0$,

$$(x-\xi) = (x - x_1 - \eta' \sin \Lambda_{LER})$$
$$(y-\eta) = (y - y_1 - \eta' \cos \Lambda_{LER})$$

and

$$R^2 = (x-\xi)^2 + \beta^2 [(y-\eta)^2 + (z-\zeta)^2]$$

$$= (x - x_1 - \eta' \sin \Lambda_{LER})^2 + \beta^2 (y - y_1 - \eta' \cos \Lambda_{LER})^2 + \beta^2 (z-\zeta)^2$$

$$= (x-x_1)^2 + \beta^2 [(y-y_1)^2 + (z-\zeta)^2]$$

$$- 2 [(x-x_1) \sin \Lambda_{LER} + \beta^2 (y-y_1) \cos \Lambda_{LER}] \eta'$$

$$+ [\sin^2 \Lambda_{LER} + \beta^2 \cos^2 \Lambda_{LER}] \eta'^2$$

Let

$$A = \sin^2 \Lambda_{LER} + \beta^2 \cos^2 \Lambda_{LER} \qquad \text{(A4a)}$$

$$B = -2 [(x-x_1) \sin \Lambda_{LER} + \beta^2 (y-y_1) \cos \Lambda_{LER}] \qquad \text{(A4b)}$$

$$C = (x-x_1)^2 + \beta^2 [(y-y_1)^2 + (z-z_1)^2] \qquad \text{(A4c)}$$

Then

$$R^2 = A \eta'^2 + B \eta' + C \qquad \text{(A5)}$$

Letting $m(\eta')$ be parabolic,

$$m(\eta') = d_0 + d_1 \eta' + d_2 \eta'^2 \tag{A6}$$

equation A2 becomes

$$\phi(x,y,z) = \int_{Y_1'}^{Y_2'} \frac{d_0 + d_1 \eta' + d_2 \eta'^2}{[A\eta'^2 + B\eta' + C]^{1/2}} \, d\eta'$$

or

$$\phi(x,y,z) = d_0 I_0 + d_1 I_1 + d_2 I_2 \tag{A7}$$

For $A \neq 0$,

$$I_0 = \int_{Y_1'}^{Y_2'} \frac{d\eta'}{[A\eta'^2 + B\eta' + C]^{1/2}}$$

$$I_0 = \frac{1}{\sqrt{A}} \ln \left| \frac{2AY_2' + B + 2\sqrt{AX_2}}{2AY_1' + B + 2\sqrt{AX_1}} \right| , \quad A > 0 \tag{A8a}$$

$$I_0 = \frac{-1}{\sqrt{-A}} \left[\sin^{-1}\left(\frac{2AY_2' + B}{\sqrt{B^2 - 4AC}}\right) - \sin^{-1}\left(\frac{2AY_1' + B}{\sqrt{B^2 - 4AC}}\right) \right] , \quad A < 0 \tag{A8b}$$

$$I_0 = \frac{1}{\sqrt{A}} \ln \left| \frac{AY_2' + B}{AY_1' + B} \right| , \quad B^2 = 4AC \tag{A8c}$$

$$I_1 = \int_{Y_1'}^{Y_2'} \frac{\eta' d\eta'}{[A\eta'^2 + B\eta' + C]^{1/2}}$$

$$I_1 = \frac{1}{A}\left[\sqrt{X_2} - \sqrt{X_1} - \frac{B}{2} I_0\right] \qquad \text{(A8d)}$$

$$I_2 = \int_{Y_1'}^{Y_2'} \frac{\eta'^2 d\eta'}{[A\eta'^2 + B\eta' + C]^{1/2}}$$

$$I_2 = \frac{1}{2A}\left\{\left(Y_2' - \frac{3B}{2A}\right)\sqrt{X_2} - \left(Y_1' - \frac{3B}{2A}\right)\sqrt{X_1} + \frac{3B^2 - 4AC}{4A} I_0\right\} \qquad \text{(A8e)}$$

where

$$X_1 = A Y_1'^2 + B Y_1' + C$$
$$X_2 = A Y_2'^2 + B Y_2' + C$$

If $X_1 < 0$, $\sqrt{X_1} \equiv 0$ and if $X_2 < 0$, $\sqrt{X_2} \equiv 0$.
For $A = 0$,

$$I_0 = \frac{2}{B}\left[\sqrt{BY_2' + C} - \sqrt{BY_1' + C}\right] \qquad \text{(A9a)}$$

$$I_1 = -\frac{2}{3B^2}\left\{(2C - BY_2')\sqrt{BY_2' + C} - (2C - BY_1')\sqrt{BY_1' + C}\right\} \qquad \text{(A9b)}$$

$$I_2 = \frac{2}{15B^3}\left\{\left[8C^2 - 4BC Y_2' + 3B^2 Y_2'^2\right]\sqrt{BY_2' + C} - \left[8C^2 - 4BC Y_1' + 3B^2 Y_1'^2\right]\sqrt{BY_1' + C}\right\} \qquad \text{(A9c)}$$

which completes the equations for calculating the line source potential.

The line source velocity components are calculated with a finite difference step as follows:

$$u = \frac{\partial \phi}{\partial x} + U_\infty = \frac{1}{\Delta X}\left[\phi(x+\Delta X, y, z) - \phi(x, y, z)\right] + U_\infty \qquad \text{(A10a)}$$

$$v = \frac{\partial \phi}{\partial y} = \frac{1}{\Delta Y}\left[\phi(x, y+\Delta Y, z) - \phi(x, y, z)\right] \qquad \text{(A10b)}$$

$$w = \frac{\partial \phi}{\partial z} = \frac{1}{\Delta Z}\left[\phi(x, y, z+\Delta Z) - \phi(x, y, z)\right] \qquad \text{(A10c)}$$

where $\Delta X = \Delta Y = \Delta Z = \bar{R}_{LE}/1000$ and $\bar{R}_{LE}$ is the average value of the leading edge radius for the line source being considered.

The coefficients, d_0, d_1 and d_2 are determined by satisfying the leading edge stagnation condition at the three locations

$$\bar{Y}_1' = Y_1' + 0.067\,(Y_2' - Y_1') \quad , \quad \bar{X}_1' = \frac{R_{LE}(\bar{Y}_1')}{\cos \Lambda_{LER}}$$

$$\bar{Y}_2' = Y_1' + 0.500\,(Y_2' - Y_1') \quad , \quad \bar{X}_2' = \frac{R_{LE}(\bar{Y}_2')}{\cos \Lambda_{LER}}$$

$$\bar{Y}_3' = Y_1' + 0.933\,(Y_2' - Y_1') \quad , \quad \bar{X}_3' = \frac{R_{LE}(\bar{Y}_3')}{\cos \Lambda_{LER}}$$

The velocity component for which stagnation is achieved is

$$u_i = U_\infty \cos \Lambda_{LER} \cos \Lambda_{LE}$$

The Mach number used in computing ϕ with equation A7 and A8 or A9 is M_∞.

Calculation of the Surface Z_S

The z_s surface used in this study is defined as that surface produced by a two dimensional line source of constant strength as required to produce a stagnation point at $x = -R_{LE}$. Thus as R_{LE} changes along the span of the wing, the surface z_s likewise changes.

The appropriate equation relating z_s and x as shown in Figure A3 is

$$z_s = \pi R_{LE} \left[1 - \frac{1}{\pi} \tan^{-1}\left(\frac{z_s}{x}\right) \right] \tag{A11}$$

for which no direct solution exists for $z_s = z_s(x)$. Approximations have been derived which are applicable in the three regions shown in Figure A3, i.e., as $x \to -R_{LE}$, $|x| \to 0$, and the remainder.

For the first region as $x \to -R_{LE}$, the inverse tangent term may be approximated as

$$\tan^{-1}\left(\frac{z_s}{x}\right) \approx \pi + \frac{z_s}{x} - \frac{1}{3}\left(\frac{z_s}{x}\right)^3$$

$$\approx \pi + \frac{\sqrt{R_{LE}^2 - x^2}}{x} - \frac{\left(R_{LE}^2 - x^2\right)^{3/2}}{3x^3}$$

Substitution into equation A11 yields

$$z_s \approx -\frac{R_{LE}}{x}\sqrt{R_{LE}^2 - x^2}\left[1 - \frac{R_{LE}^2 - x^2}{3x^2}\right] \tag{A12}$$

for $-R_{LE} \leq x \leq -.98 R_{LE}$.

For $|X| \to 0$, equation A11 is rewritten as

$$z_s = X \tan\left[\pi - \frac{z_s}{R_{LE}}\right] \tag{A13}$$

At $X=0$, $z_s = \pi R_{LE}/2$, thus the tangent term may be approximated as

$$\tan\left[\pi - \frac{z_s}{R_{LE}}\right] \approx \frac{1}{\frac{z_s}{R_{LE}} - \frac{\pi}{2}}, \quad X \sim 0$$

Now

$$z_s \approx \frac{X}{\frac{z_s}{R_{LE}} - \frac{\pi}{2}}$$

or

$$\frac{z_s^2}{R_{LE}} - \frac{\pi z_s}{2} - X = 0$$

which yields

$$z_s = \frac{\pi R_{LE}}{4} + \frac{R_{LE}}{2}\sqrt{\frac{\pi^2}{4} + \frac{X}{R_{LE}}} \tag{A14}$$

for $|X| \leq 0.1 R_{LE}$.

The remaining regions, $-0.98 R_{LE} < X < -0.1 R_{LE}$ and $X > 0.1 R_{LE}$ are treated with a combined approximation and iteration scheme. Starting with equation A13, the following approximation is made for z_s as

$$\frac{z_s}{\pi R_{LE}} \approx \frac{z_s^*}{\pi R_{LE}} = 1 - e^{-n(x + R_{LE})}$$

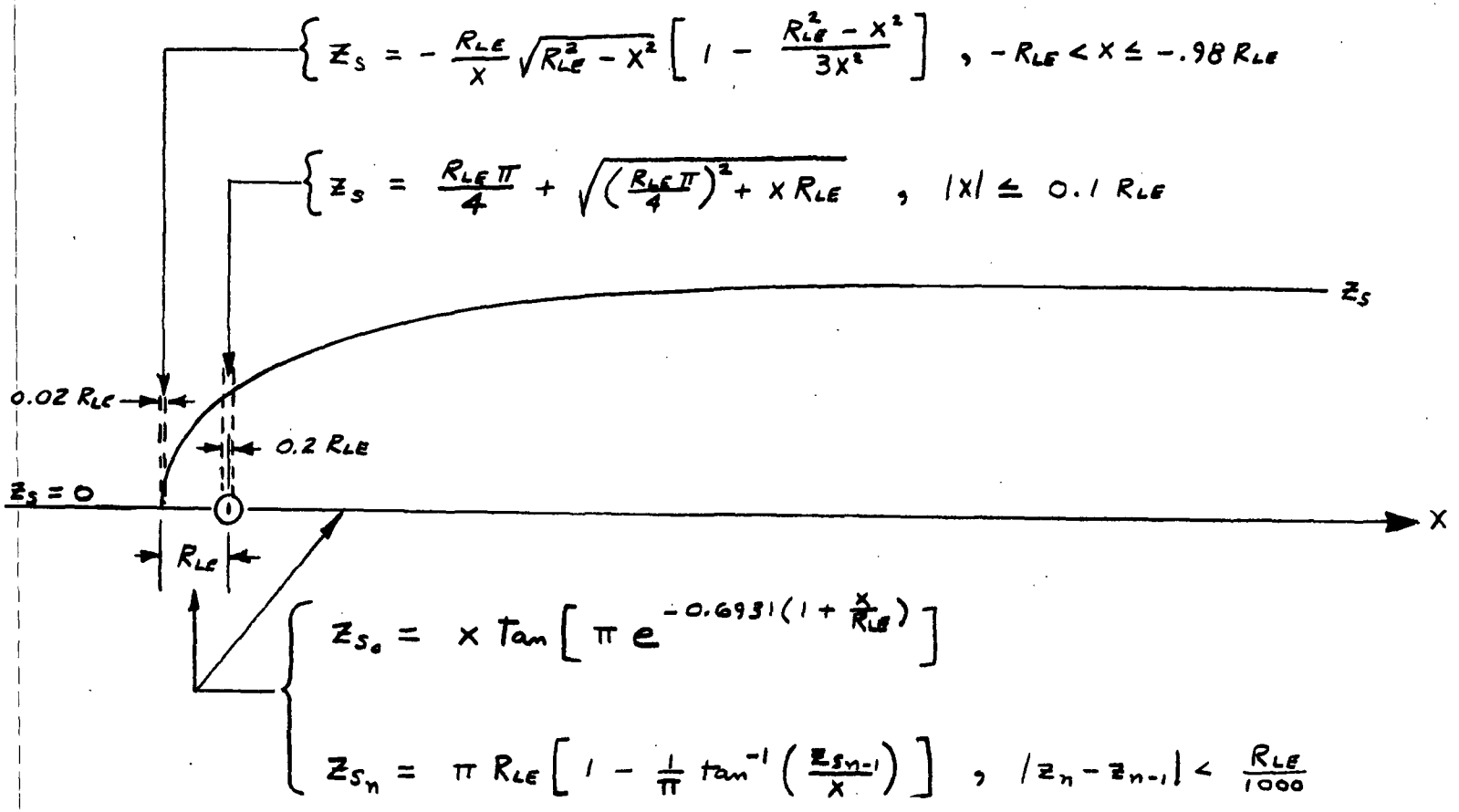

Figure A3.- Equation summary for calculating Z_S

The coefficient n is chosen so that

$$z_s^* = z_s \quad @ \quad x = -R_{LE}, 0, \infty$$

At $x=0$, $z_s = \pi R_{LE}/2$, thus

$$\frac{1}{2} = 1 - e^{-n R_{LE}} \Rightarrow n = \frac{1}{R_{LE}} \ln(2) = \frac{0.6931}{R_{LE}}$$

Now equation A13 becomes

$$z_{s_0} = x \tan\left[\pi - \pi\left(1 - e^{-0.6931\left(1 + \frac{x}{R_{LE}}\right)}\right)\right]$$

or

$$z_{s_0} = x \tan\left[\pi e^{-0.6931\left(1 + \frac{x}{R_{LE}}\right)}\right] \tag{A15}$$

The i^{th} approximation is calculated as

$$z_{s_i} = \pi R_{LE}\left[1 - \frac{1}{\pi}\tan^{-1}\frac{z_{s_{i-1}}}{x}\right] \tag{A16}$$

which is iterated until $|z_{s_i} - z_{s_{i-1}}| < R_{LE}/1000$.

Slopes are calculated in all regions except $|x| \leq 0.1 R_{LE}$ as

$$\left(\frac{\partial z_s}{\partial x}\right)_x = \left(\frac{\Delta z}{\Delta x}\right)_x = \frac{z_{s_2} - z_s}{x_2 - x} \tag{A17a}$$

where

$$z_{s_2} = z_s + \frac{\pi R_{LE}}{1000} < 0.98\,\pi R_{LE} \tag{A17b}$$

and

$$x_2 = \frac{z_{s_2}}{\tan\left[\pi - \frac{z_{s_2}}{R_{LE}}\right]} \tag{A17c}$$

If $z_{s_2} \geq .98\pi R_{LE}$, let

$$z_s \approx \pi R_{LE}\left[1 - \frac{z_s}{\pi x}\right]$$

thus

$$z_s \approx \frac{\pi R_{LE}}{1 + \frac{R_{LE}}{x}}$$

for which the slope is

$$\left(\frac{\partial z_s}{\partial x}\right)_x \approx \frac{\pi}{1 + \frac{2x}{R_{LE}} + \left(\frac{x}{R_{LE}}\right)^2} \qquad \text{(A18)}$$

for $z_{s_2} \geq .98\pi R_{LE}$. In the region $|x| \leq 0.1 R_{LE}$, the slope is calculated as

$$\left(\frac{\partial z_s}{\partial x}\right)_x = \frac{R_{LE}}{4\sqrt{\frac{\pi^2}{4} + \frac{x}{R_{LE}}}} \qquad \text{(A19)}$$

which completes the equations for slopes of z_s.

Velocity Components on Z_S

Since the aerodynamic solution is performed along the surface z_s, the normal and tangential velocity components are needed. Referring to Figure A4, the velocity components in the x and z directions are u and w and the tangential and normal velocities are $\bar{u}$ and $\bar{w}$.

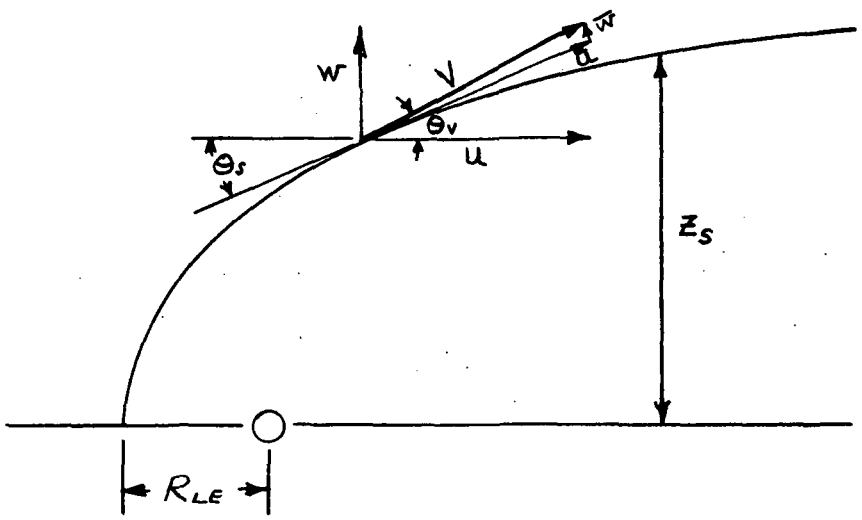

Figure A4.- Tangential and normal velocities on surface Z_s

The total velocity is

$$V^2 = u^2 + w^2 \tag{A20a}$$

where u and w are defined in equations (A10a) and (A10b), and the angle θ_v is

$$\theta_v = \tan^{-1}\left(\frac{w}{u}\right) \tag{A20b}$$

Thus $\bar{u}$ and $\bar{w}$ are

$$\bar{u} = V \cos(\theta_v - \theta_s) \tag{A20c}$$

$$\bar{w} = V \sin(\theta_v - \theta_s) \tag{A20d}$$

where θ_s is obtained as

$$\theta_s = \tan^{-1}\left(\frac{\partial z_s}{\partial x}\right)_x \tag{A20e}$$

from equations A17, A18, or A19.

Generally, $\bar{w}$ is non zero since z_s is defined for two dimensional flow. Also, due to the use of the local linearization concept, the velocities are calculated according to the local Mach number, which will differ from those calculated with M_∞.

Exact Isentropic Relations Used in Computing C_p, M_ℓ and $\bar{u}_\ell$

For a given value of $\bar{u}$ as calculated from the above equations for the leading edge line source, the pressure coefficient, C_p, is calculated as

$$C_p = \frac{2}{\gamma M_\infty^2}\left\{\left[1 + \frac{\gamma-1}{2} M_\infty^2\left(1 - \frac{\bar{u}}{U_\infty}\right)\right]^{\gamma/\gamma-1} - 1\right\} \tag{A21}$$

The local Mach number, M_ℓ, is calculated for a given C_p as

$$M_\ell = \left\{\frac{1}{\gamma-1}\left[\frac{2 + (\gamma-1) M_\infty^2}{\left(1 + \frac{\gamma M_\infty^2 C_p}{2}\right)^{\frac{\gamma-1}{\gamma}}} - 2\right]\right\}^{1/2} \tag{A22}$$

The tangential velocity, $\bar{u}_\ell$, for a given M_ℓ is calculated as

$$\bar{u}_\ell = \frac{M_\ell U_\infty}{M_\infty}\left[\frac{2 + (\gamma-1) M_\infty^2}{2 + (\gamma-1) M_\ell^2}\right]^{1/2} \tag{A23}$$

REFERENCES

1. Cunningham, A. M., Jr.: A Steady and Oscillatory Kernel Function Method for Interfering Surfaces in Subsonic, Transonic, and Supersonic Flow. NASA CR-144895, Sept. 1976.

2. Kolbe, C. D.; and Boltz, F. W.: The Forces and Pressure Distribution at Subsonic Speeds on a Plane Wing Having 45° of Sweepback, an Aspect Ratio of 3, and a Taper Ratio of 0.5. NACA RM A51G31, Oct. 1951.

3. Schlichting, H.: Boundary Layer Theory. McGraw-Hill Book Co., Inc., New York, 1960.

4. Magnus, R.; Yoshihara, H.: Finite Difference Calculations of the NACA 64A-410 Airfoil Oscillating Sinusoidally in Pitch at M_∞=0.72. CASD-NSC-74-004, Aug. 1974.